
Article:
Forster, L. orcid.org/0000-0001-6159-6360, Kashbor, M.M.M., Railton, J. orcid.org/0000-0002-4194-3799 et al. (4 more authors) (2023) Low-field 2D NMR relaxation and DRIFTS studies of glucose isomerization in zeolite Y: new insights into adsorption effects on catalytic performance. Journal of Catalysis, 425. pp. 269-285. ISSN 0021-9517

https://doi.org/10.1016/j.jcat.2023.06.021

Journal of Catalysis 425 (2023) 269–285

Contents lists available at ScienceDirect

Journal of Catalysis

journal homepage: www.elsevier.com/locate/jcat

Research article

Low-field 2D NMR relaxation and DRIFTS studies of glucose isomerization in zeolite Y: New insights into adsorption effects on catalytic performance

Luke Forster [a,*], Mohamed M.M. Kashbor [b], James Railton [b], Sarayute Chansai [a], Christopher Hardacre [a], Marco Conte [b,*], Carmine D'Agostino [a,c,*]

[a] Department of Chemical Engineering, The University of Manchester, Oxford Road, Manchester M13 9PL, United Kingdom
[b] Department of Chemistry, University of Sheffield, Sheffield S3 7HF, United Kingdom
[c] Dipartimento di Ingegneria Civile, Chimica, Ambientale e dei Materiali (DICAM), Alma Mater Studiorum – Università di Bologna, Via Terracini, 28, 40131 Bologna, Italy

ARTICLE INFO

Article history:
Received 15 December 2022
Revised 19 March 2023
Accepted 14 June 2023
Available online 17 June 2023

Keywords:
Glucose to fructose isomerization
Zeolites
NMR relaxation
Green solvents
IR

ABSTRACT

Sn and Ga doped zeolite Y catalysts were tested for the isomerization of glucose to fructose carried out in different solvents (water, methanol and ethanol). Therein, ethanol favoured a Lewis acid site catalyzed pathway that promotes glucose isomerization to fructose, whereas methanol resulted in an equal distribution of products (mannose, fructose and alkyl fructoside). In contrast, the catalysts were totally inactive in water solvent. NMR relaxation measurements, including solvent displacement experiments, suggested that the lack of catalytic activity in water is due to the strong adsorption of this solvent within the zeolite pores blocking reactants from the Lewis acid sites active for the sugar isomerization. In comparison, ethanol adsorbs relatively more strongly than methanol, hence is retained in the pores where solvated fructose is preferentially prevented from the further reaction on Brønsted acid sites situated outside of the pore space. NMR relaxation measurements using pyridine and tetrahydrofuran (THF) and pyridine-DRIFTS measurements suggest metal doping had little effect on the overall relative acid strength of the zeolites but resulted in zeolites with increased Lewis acid strength relative to the non-doped zeolites. The results reported provide direct experimental evidence on the importance of adsorption properties of solvents within zeolites used for glucose to fructose isomerization and may serve as a starting point for a new approach towards designing and optimizing such catalytic systems.

1. Introduction

In recent times, the development of manufacturing processes with minimal environmental impact has become of paramount importance to academic and industrial researchers alike. This is due to rapidly increasing levels of waste and the subsequent environmental concerns raised. [1] As such, green and sustainable chemistry has become one of the most important concepts to combat climate change and environmental damage. Green chemistry is a broad and far-reaching concept defined by twelve key principles; one of which is catalysis. [2] The role of catalysis in green chemistry lies in its ability to increase the efficiency of chemical manufacturing systems by reducing the energetic footprint and the production of waste products [3–5] or potentially allowing new, sustainable feedstocks or fuels to be used in chemical processes that were previously not viable. [6–8]

As crude oil stocks are depleting it is vital that new sustainable alternatives are discovered. One promising alternative route to renewable biofuels is through the valorization of biomass. [9–10] Biomass is generally comprised of carbohydrates, proteins, lipids and fatty acids and it is through the breakdown of these compounds that high value platform chemicals can be produced. For example, for use as versatile building blocks to form useful products, such as fuels and chemical monomers. [11–14] 5-Hydroxymethlfurfural (HMF) is one such industrially desirable platform chemical that can be derived from carbohydrates and used to produce a wide range of important building block chemicals such as 2,5-furandicarboxylic acid [15–17] and 2,5-dimethylfuran [18–20] or even levulinic acid, which has been pre-

* Corresponding authors at: Department of Chemical Engineering, The University of Manchester, Oxford Road, Manchester M13 9PL, United Kingdom (Carmine D'Agostino); Department of Chemistry, University of Sheffield, Sheffield S3 7HF, United Kingdom (Marco Conte).

E-mail addresses: luke.forster@manchester.ac.uk (L. Forster), marco.conte@sheffield.ac.uk (M. Conte), carmine.dagostino@manchester.ac.uk, carmine.dagostino@unibo.it (C. D'Agostino).

https://doi.org/10.1016/j.jcat.2023.06.021
0021-9517/

viously recognized as one of the top twelve building blocks that can be derived from biomass feedstock.[21]

The utility of biomass as a renewable feedstock used to produce high-value platform chemicals is critically dependent on the efficient conversion of cellulosic matter. Pentose (C5) sugars, such as xylose, have been suggested as appropriate molecules for this process due to a high atom efficiency when converting to levulinic acid [22–23] but the formation of insoluble, undesired side products such as humins can lead to catalyst poisoning, [24–25] thereby decreasing the viability of the overall process. Hexose (C6) sugars, like glucose, have also been considered, as glucose is efficiently produced by the hydrolysis of cellulose. [26–27] Therefore, it is cheap and highly abundant. However, glucose is a relatively inert molecule due to its stable 6-membered ring structure, and the subsequent dehydration of glucose to 5-HMF is a relatively inefficient process. [28] As such, fructose has been suggested as an alternative, as its 5-membered ring structure is both more reactive and more prone to undergoing the efficient dehydration step *via* enolization of the open chain saccharide. [29–30] However, fructose is much less abundant than its isomer glucose and finds much use in the food and drink industry as a sweetener [31–32] resulting in a higher relative cost (722 USD/ton) [33] of fructose compared to 300 USD/ton for glucose). [34] Therefore, it is vital to find efficient processes for the conversion of glucose to fructose.

Currently, a promising catalyst reported for the glucose to fructose isomerization reaction is a Sn doped beta zeolite, which gives yields of 31 wt% fructose and 9 wt% mannose, and a 46 wt% of unreacted glucose after various reaction times within the temperature range 343 K to 413 K. [35] The Sn beta zeolite possesses two separate types of active sites, the "closed" form and "open" form corresponding to non-hydrolyzed, fully coordinated Sn sites and partially hydrolyzed Sn sites, respectively, [36] with the open site being the most catalytically active. [37] However, the reaction is shown to occur more readily in methanol than in water as the Sn beta zeolites possess hydrophobic micropores, thereby allowing a greater uptake of methanol solvent as opposed to water [38–39] giving rise to a partial solvation of the sugar-catalyst complex during the reaction and thereby increasing catalytic activity [28].

Our recent work has shown that Sn and Ga doped zeolite Y catalysts exhibit similar behaviour in water, but have also been shown to be active for the conversion of glucose to its isomerization products (namely, fructose and mannose) in methanol. However, large amounts of alkyl fructoside intermediate are also produced in approximately equal amounts. [40] Interestingly, relatively large amounts of fructose are produced (yield ca. 50 %) when water is introduced after a reaction in methanol in a two-step solvent protocol. This effect is attributed to a change in reaction mechanism based on the solvent used. [40] This is in good agreement with previous, earlier work based on the use of zeolites for the conversion of glucose to fructose in consecutive reactions in alcohol and aqueous media. [41].

Solvent effects are widespread in the field of heterogeneous catalysis, but relatively little work has been carried out to determine the processes occurring between the reactive species present and the active sites on the surface of the catalyst within the catalyst pore. In this context, NMR relaxation measurements represent a valuable tool to provide vital information on phenomena occurring within the porous structure of catalytic materials. Indeed, it has been shown that NMR relaxation time measurements can be used to characterize the adsorption strengths of reactants with a given catalyst surface. [42] By comparison of these adsorption strengths for both the reactant and solvents, the solvent effects seen in the liquid phase oxidations of both 1,4-butanediol to γ-butyrolactone [43–44] and various propanediols to their respective carboxylic acid and methyl ester analogues [45] have been explained using NMR relaxation measurements and therefore the optimal solvent/conditions in which to carry out these reactions can be identified. Solvent effects in catalytic processes involving polyalcohols are of particular relevance to this work, as glucose, fructose and mannose each contain multiple hydroxyl group functionalities.

Additionally, NMR relaxation measurements have shown that 1,4-dioxane interacts strongly with sites on the surface of TiO_2 support *via* oxygen lone electron pairs, thereby inhibiting access of reactive species to catalytically active sites on the catalyst surface and showing that non-oxygenated solvents such as cyclohexane are preferable for reactions using TiO_2 supported catalysts. [46] NMR relaxation measurements have also proven to be an effective tool for measuring the acidity of catalytic materials [47] which is often vital to their performance for certain reactions *i.e.* sugar isomerization. Furthermore, 2D NMR measurements have been shown to be a valuable method to characterize sorption in microporous materials. [48–50] It is important to consider, however, that solvent effects have been shown to impact sugar isomerization reactions in more ways than just the blocking of catalytically active sites. In fact, recent work has shown that solvents are important in controlling both the concentration and entropy of the solvated sugar. [51–52].

In this work, Sn and Ga doped zeolite Y catalysts have been synthesized and shown to effectively isomerize glucose to produce relatively high yields of fructose and mannose. The effect of the reaction solvent upon the overall catalytic activity and mechanism of the system has been evaluated using NMR relaxation measurements to aid the optimization of the catalytic system. Finally, an unconventional combined pyridine/THF-NMR relaxation and *in-situ* pyridine-DRIFTS investigation was carried out to effectively characterize the acidity of the zeolites studied and relate these characteristics to their catalytic performance.

2. Experimental

2.1. Materials

Materials were used as received, without any additional purification, unless otherwise specified. Metal precursors: $Ga(NO_3)_3{\cdot}xH_2O$ (Acros, Ga assay 25 wt%), $SnCl_4{\cdot}5H_2O$ (Fisher, Sn assay 34 wt%); supports: zeolite Y (Zeolyst International, CBV720 molar SiO_2:Al_2O_3 = 30), γ-Al_2O_3 (Alfa Aesar, 99.997%), silica fumed SiO_2 (Aldrich, 99.8%); metal oxides: β-Ga_2O_3, (Acros, > 99.99%) and SnO_2 (Acros, 99.9%); sugars: glucose (D-(+)-glucose, Alfa Aesar, anhydrous, 99%), fructose (Fisher, > 99%), mannose (D-(+)-mannose, Alfa Aesar, > 99 %), methyl fructoside (methyl β-D-fructofuranoside, MuseChem, 98%); solvents: methanol (Fisher, HPLC Grade, > 99.9%), ethanol (Sigma, > 99%, anhydrous, ≤ 0.005% water), pyridine (Sigma, anhydrous, >99.9%), tetrahydrofuran (ThermoFisher, anhydrous, > 99.9%). Deionized water was obtained using a Elgastat Option 3B unit with a conductivity of 1 MΩ cm^{-1} at neutral pH. Additional specifications are: organics < 0.001 AU at 254 nm, TOC < 50 ppb, bacteria < 1 cfu mL^{-1}.

2.2. Catalyst preparation

Ga and Sn doped zeolite Y catalysts, herein reported as Ga/Y and Sn/Y, respectively, were prepared using a wet impregnation protocol with water as the solvent for the dissolution and impregnation of metal precursors into the zeolite. [53] Zeolite Y was used in its acidic form, herein reported as HY. The metal precursors used to prepare Ga/Y and Sn/Y were $Ga(NO_3)_3{\cdot}xH_2O$, and $SnCl_4{\cdot}5H_2O$, respectively.

The catalysts were prepared with a final metal loading of 1 wt% and the desired amount of metal precursor (59.1 mg and 78.5 mg for $SnCl_4{\cdot}5H_2O$, and $Ga(NO_3)_3{\cdot}xH_2O$, respectively) was dissolved in water (25 mL) and mixed with zeolite Y (ca. 2 g) under vigorous stirring. The amount of zeolite was adjusted to compensate for the metal assay for each precursor (zeolite HY 1.98 g). The resulting slurry was heated up slowly to 80 °C and evaporated to dryness. Each catalyst was then dried at 120 °C for 16 h and calcined at 550 °C for 4 h in static air (temperature ramp 20 °C min^{-1}).

Catalysts used for control tests (Sn/SiO_2, Sn/Al_2O_3, Ga/SiO_2 and Ga/Al_2O_3) were prepared using an identical protocol to the one described using HY above, but by using SiO_2 and γ-Al_2O_3 as supports.

2.3. Catalytic testing

The catalyst was dispersed in solutions containing 4 mL of water, methanol or ethanol and 125 mg of glucose (α-D-glucose). The amount of catalyst, ca. 75 mg for zeolite HY, was adjusted to a molar metal to glucose ratio of 1:100 with respect to the total amount of Sn or Ga in the zeolite (83 and 47 mg for Sn/Y and Ga/Y zeolites, respectively, for a 2 g batch).

Unless otherwise specified, the catalytic tests were carried out in a sealed pressure tube (Ace-type GPE Scientific) at a reaction temperature of 100 °C and reaction time of 1 h. The tube containing the reaction mixture was inserted into a pre-heated, temperature calibrated, aluminium block for the desired reaction time and equipped with a magnetic stirrer operating at 700 rpm. After the desired reaction time, the reaction mixture was quickly cooled down to room temperature by immersing the pressure tube in an ice bath.

2.4. Analysis of reaction mixtures

High performance liquid chromatography was used for the characterization of the reaction mixtures, using a Shimadzu UFLC XR chromatograph. A method for a fine resolution of the reaction mixture and identification of impurities made use of a Phenomenex Rezex RCM-Monosaccharide Ca++ column 300 × 7.8 mm with a column temperature of 60 °C and a mobile phase consisting of purified water running an isocratic elution program at a flow rate of 0.6 mL min^{-1} over 25 min and injection volume of 10 μL. The HPLC apparatus was equipped with an evaporative light scattering detector (ELSD) and the respective sugar concentrations were calculated with respect to external standards against calibration plots. Conversion and selectivity were calculated as defined in Equations S1-S8.

2.5. NMR relaxation 2D T_1-T_2 correlation analysis

3 mm thick pellets of non-doped and Ga or Sn doped zeolite Y were soaked in *n*-octane, deionized water, methanol or ethanol for 2 days prior to analysis. The zeolites were removed from the respective liquids and gently dried on a filter paper pre-soaked with the same liquid as used for the absorption to remove excess liquid from the outer surface whilst avoiding the removal of liquid from the internal pore structure.

Following drying, the zeolites were transferred to 5 mm NMR tubes and tested using a T_1-T_2 NMR pulse sequence (Figure S1) to determine spin–lattice and spin–spin relaxation times. The typical experimental error for all T_1-T_2 measurements was approximately 3 %.

Sixteen recovery delays were used from 1 ms to 500 ms. The echo train of the CPMG sequence was composed of 1200 or 1600 echoes (dependent upon the sample) and acquired in a single shot with an echo spacing of 2τ = 1 ms. Each data set was acquired with 4 scans in approximately 2 min.

NMR relaxation experiments were performed using a Magritek SpinSolve benchtop NMR spectrometer operating at a ^1H frequency of 43 MHz. The 2D data was processed using an algorithm kindly provided by Prof. Michael Johns of the University of Western Australia, Perth.

See Section 3 of the Supporting Information for a more detailed description of the principles of the NMR relaxation measurements used.

2.6. NMR relaxation 2D T_1-T_2 correlation displacement experiments

3 mm thick pellets of non-doped and Ga or Sn doped zeolite Y were soaked in methanol or ethanol for 2 days prior to analysis. The large zeolite grains were removed from the liquid before being dried, prepared and analysed using the same process detailed previously. The large zeolite grains were then removed from the NMR tube and left in an excess of the displacing liquid (water) for the amount of time specified, herein referred to as the displacement time. The excess liquid was again removed prior to the acquisition of the NMR data using the process detailed previously to obtain a 2D T_1-T_2 correlation plot for varying values of the displacement time.

2.7. Pyridine diffuse reflectance infrared Fourier transform spectroscopy (DRIFTS)

In-situ DRIFTS measurements were performed using a Bruker Vertex 70 FTIR spectrometer equipped with a mercury-cadmium-telluride, liquid N_2-cooled detector. Approximately 25 mg of the catalyst sample of interest was placed in a ceramic crucible in the DRIFTS cell. Prior to the experiments, the catalyst was pre-treated to remove moisture by heating in Ar with a total flow rate of 50 cm^3 min^{-1} up to 400 °C for 1 h and then cooled down in flowing Ar to 35 °C. The IR spectrum of the catalyst at 35 °C under flowing Ar was taken as a background.

Pyridine adsorption was carried out at 35 °C using pyridine vapour obtained using a saturator and Ar flow as a carrier gas. The pyridine saturator was placed in an ice/water bath to obtain a pyridine concentration of 2000 ppm. The total flow rate was 50 cm^3 min^{-1}. After 60 min, pyridine was purged for 30 min using Ar to remove weakly adsorbed pyridine from the catalyst surface. The temperature of the DRIFTS cell was then increased in increments of 50 °C up to 350 °C and *in-situ* DRIFTS spectra were acquired at each increment (50 °C, 100 °C, 150 °C, 200 °C, 250 °C, 300 °C, 350 °C).

In all cases, the *in-situ* DRIFTS spectra were recorded with a resolution of 4 cm^{-1} and with the accumulation of 128 scans every 60 s during transient switches. The DRIFTS spectra were analyzed using the OPUS software. The IR data are reported as log 1/*R* ("absorbance"), with $R = I/I_0$, where *R* is the sample reflectance, *I* is the intensity measured under reaction conditions, and I_0 is the intensity measured on the pure catalyst powder under a flow of Ar at 35 °C.

2.8. XRPD

X-ray powder diffraction (XRPD) patterns were acquired using a Bruker D8 Advance equipped with a LynxEye detector. The samples were measured over an amorphous silicon sample holder. The instrument was operating at 40 kV and 40 mA selecting CuK αradiation as the X-ray source. The samples were analyzed in the range 5° to 80° 2θ for a scan time of 70 min. Analysis of the patterns was carried out using the X-Pert Pro software.

In order to determine unit cell parameters, the powder X-ray patterns were fitted by using a Rietveld refinement [54] as a full-pattern fit algorithm for each sample. The goodness of fit between experimental and simulated XRPD patterns was evaluated *via* a χ^2-test. [55] Crystallographic information files (CIF) from the Database of Zeolite Structures (IZA-SC) [56] were used to obtain the atomic coordinate values needed to carry out the fitting.

2.9. ICP-MS

Determination of Sn and Ga content was carried out *via* inductively coupled plasma-mass spectrometry (ICP-MS) analysis using an Agilent 7500CE ICP-MS instrument calibrated up to 10 parts per billion (ppb) using standards prepared by dilution from stock solutions containing 1000 parts per million (ppm) of Ga or Sn standards. The concentrations of Ga and Sn in the samples were calculated against a calibration graph.

2.10. BET surface area and porosimetry

The textural properties of the catalysts were determined using a Micromeritics 3Flex Analyzer Gas Sorption System operating at liquid nitrogen temperature. The typical amount of zeolite for the measurement was 100 mg, and the samples were degassed under vacuum at 180 °C for 48 h before being analysed. Both the adsorption and desorption branches were collected, and the Brunauer–Emmett–Teller (BET) model was used to calculate the specific surface area from the BET absorption isotherm using 0.162 nm^2 as the surface area for gaseous N_2. [57]. The hysteresis cycles were used to determine the isotherm type and the external and microporous areas of the zeolites. t-plots were used to determine the pore volume, with a Barrett-Joyner-Halenda (BJH) procedure for the determination of the pore distribution, [58] and the use of a Horvath-Kawazoe model [59] for the fine fitting of the diameter of the microporous component of the zeolite Y framework.

3. Results and discussion

3.1. Catalytic testing

Both the metal doped and non-doped zeolites were tested for the conversion of glucose to its isomerization products, fructose and mannose. The reaction solvent is known to play a significant role in heterogeneous catalytic reactions, as discussed previously, by influencing factors such as the adsorption of reactive species, [43–45] the solubility of reagents [51,60] and by directly influencing the catalytic cycle through interactions with species involved in the catalytic cycle. [61] As a consequence, to investigate potential solvent effects for our catalytic systems, the reactions using each catalyst were carried out using water, methanol or ethanol as the reaction solvent.

For the reactions using water as the reaction solvent, no conversion of glucose was observed. Previous work has shown that the use of water as a solvent for reactions using a zeolite catalyst with relatively hydrophilic pores can result in a significant decrease in catalytic activity. [30] This detrimental effect is likely due to water entering and filling the pores of the zeolite, in such a way as to prevent the entrance of sugar molecules into the pore and therefore prevent the reaction. On the other hand, a high Lewis acidity - with Lewis acid sites situated inside the pores of the zeolite, which is one of the key features to explain the reactivity of zeolites - may actually be counterproductive if strong coordination of water to Lewis acidic sites *via* electron-rich oxygen atoms occurs, as this would be hindering coordination of reactive species hence suppressing catalytic activity. [29].

Unlike the reactions in water, the reactions in alcohol solvents, namely methanol and ethanol, resulted in the conversion of glucose to fructose, mannose and an alkyl fructoside (Fig. 1 and Table S1), with the latter being either a methyl fructoside or an ethyl fructoside, respectively.

Using non doped HY as the catalyst for this reaction at 100 °C showed glucose conversions of approximately 90 % in methanol. This is greater than often reported conversion values in the literature, which are seen to convert only ~ 40 % of glucose. [60] Herein, the presence of products other than the isomerization products mannose and fructose is attributed to the formation of alkyl fructoside intermediates due to a Brønsted acid catalyzed reaction pathway (Scheme 1) between fructose and the alcohol solvent. The chemical structure of the reactants/products used in this reaction are shown in Fig. 2. Doping of HY with Sn and Ga metals showed little improvement in the overall glucose conversion seen (92 % and 93 %, respectively) in methanol.

Although the three porous materials HY, Sn/Y and Ga/Y (Table S1 and S2) do show similar results in each solvent (Fig. 1), it is important to underline that we are investigating the difference between each catalyst in the different solvents to identify common trends that can explain the observed reactivity. In fact, the similarities in reactivity of the three catalysts within the same solvents are diagnostic of a reaction mechanism dominated by Brønsted acid sites leading to the formation of an alkyl fructoside intermediate.

Consequently, although the metal dopant can, in principle, affect the Lewis acidity of our materials, Brønsted acid sites must be considered too. The activity will be a result of fine tuning between sites inside the pores of the zeolites and acidic centres outside the pores of the zeolite crystals. Therefore, the final and net effect on catalytic activity will be difficult to accurately predict. As discussed previously, when a Sn/zeolite beta catalyst was used for this reaction, a similar solvent effect was also seen for the glucose isomerization in that the catalytic activity is enhanced when methanol solvent is used as opposed to water. [38–39] This occurs due to increased uptake of methanol, relative to that of water, into the zeolite pores which are relatively less hydrophilic than the external surface of the zeolite crystals. This leads to increased solvation, and, therefore, probable stabilization of a pre-reactive sugar-catalyst complex intermediate within the zeolite pores. [28,52] In ethanol, the conversion obtained using all catalysts was practically 100 % within experimental error indicating that, in terms of total conversion, ethanol is the optimal solvent for this system, though with a distinct product distribution.

In fact, when the product yields are considered (Table S2), in methanol there is an approximately equal distribution of products (fructose, mannose and methyl fructoside) obtained, though with a slight preference for methyl fructoside (ca. 30 % – 35 %). Conversely, when ethanol is used as the reaction solvent, the order of product yield is reversed and fructose is produced as the major product (ca. 53 % – 65 %). Our previous work has suggested that the product distribution in this reaction is the result of three concurrent mechanisms (Scheme 1). [40].

When Scheme 1 is considered in relation to the catalytic data, the Brønsted acid mediated conversion of fructose to alkyl fructoside is far more prevalent when methanol is used as a reaction solvent compared with ethanol. In fact, due to the approximately equal product distribution when methanol is used, it can be assumed that all pathways are equally dominant, with the exception of the reverse reaction converting fructose to glucose. Conversely, the Lewis acid mediated isomerization is the dominant mechanism when ethanol is used as the reaction solvent.

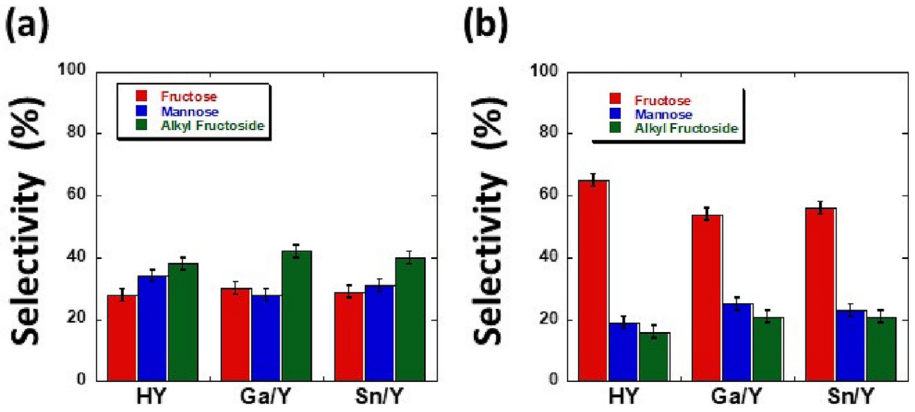

Fig. 1. Product selectivity obtained from the glucose isomerization reaction at 100 °C and endogenous pressure, using HY, Ga/Y and Sn/Y catalysts in (a) methanol and (b) ethanol solvent for a reaction time of 1 h. Total glucose conversion was *ca.* 90 % in methanol and ca. 100 % in ethanol.

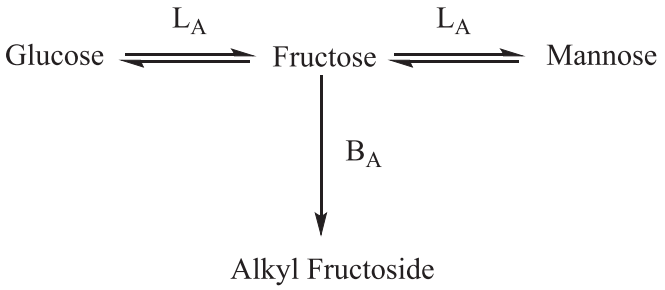

Scheme 1. The concurrent mechanisms occurring in the catalytic isomerization of glucose in alcohol media. The overall catalytic process is composed of the reversible isomerization reactions of glucose to fructose and fructose to mannose mediated by catalytic Lewis acid sites and the Brønsted acid centres, with the former responsible for the isomerization reaction, and the latter for the addition of a methoxy group to the sugar. L_A and B_A indicate Lewis and Brønsted acid mediated pathways, respectively.

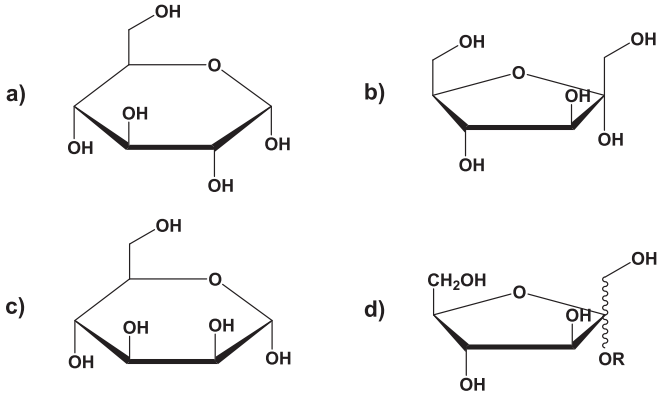

Fig. 2. The chemical structures of: (a) α-D-glucose, (b) α-D-fructose, in its furanose form, (c) α-D-mannose and (d) alkyl fructofuranoside (either α or β form) where R = CH_3– for a reaction carried out in methanol and CH_3-CH_2– for a reaction carried out in ethanol.

3.2. Solvent 2D T_1-T_2 NMR relaxation

In view of the obtained catalytic activity data and proposed solvent-dependent reaction mechanisms, T_1-T_2 measurements were performed to assess the relative interaction strengths of the reaction solvents used (water, methanol and ethanol) with the surface of the various catalysts. *n*-Octane was used as a reference guest molecule with little to no interaction with the zeolite surface, owing to its lack of chemical functionality. NMR relaxation measurements have been shown to be an effective measure of interaction strengths of fluids confined in porous media with the surface of the porous medium in question. [43–45] Previous work has shown that T_1/T_2 is related to the strength of surface adsorption and can be directly correlated to adsorption energies determined using temperature programmed desorption (TPD). [42] That is, a high value of T_1/T_2 is indicative of a high strength of interaction between a probe molecule and the surface of the porous medium within which the probe molecule is confined.

It is important to note that T_1/T_2 can be significantly impacted by factors other than surface adsorption/interaction strength, namely molecular diffusion and confinement effects. [62] The influence of molecular diffusion on the measured value of T_2 and subsequently T_1/T_2, is strongly dependent upon the presence of internal field gradients within the material under study. [63] However, such effects can be considered negligible at low external magnetic fields, [64] such as that used in this study (43 MHz), hence diffusion effects are not considered to influence the reported results. Similarly, confinement effects are only significant when the pore size is approximately equivalent to the molecular dimensions of the probe molecule, that is, mass transport is defined by configurational diffusion. [65] This is not the case in our study; therefore, it is reasonable to assume that trends in T_1/T_2 are related solely to the strength of probe molecule adsorption. As such, T_1/T_2 is a useful parameter in the field of catalysis and surface science used to characterize the strength of surface interactions of fluid/-solid interfaces in porous materials and explain phenomena such as solvent effects. [43–45].

The 2D T_1-T_2 correlation maps obtained can be seen in Fig. 3. It should be noted that 2D T_1-T_2 experiments reported in this work are based on *time domain* NMR measurements and as such, no spectral data are involved. See Section 3 of the Supporting Information for a more detailed description of the principles of the NMR relaxation measurements used.

From T_1/T_2, as previously discussed, it is possible to determine the relative strengths of surface interactions for the solvent imbibed within HY used as a benchmark. Water has $T_1/T_2 \approx 7.1 \pm 0.2$ indicating that this is the most strongly adsorbed of the solvents tested in this study and this relatively strong adsorption could be responsible for the solvent effect observed in the isomerization of glucose. This is expected, as the water molecules can strongly interact with any OH groups present on the zeolite surface, with the net result of practically occluding the pores of the zeolite to a potential substrate. When ethanol and methanol are used, the T_1/T_2 decreases significantly compared with that found for water with the zeolite surface, showing a slight preference for

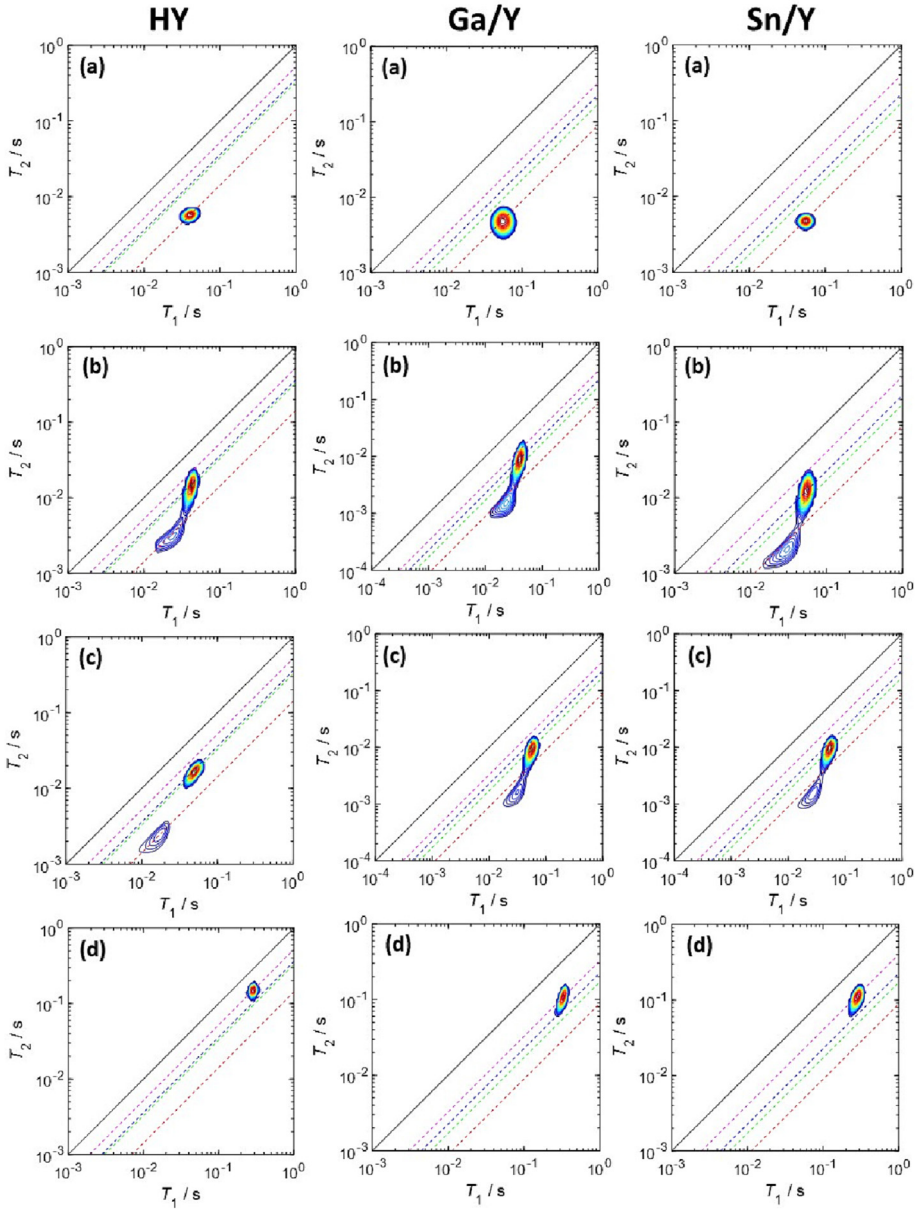

Fig. 3. T_1-T_2 relaxation correlation plots for (a) water, (b) methanol, (c) ethanol and (d) *n*-octane imbibed within the pores of HY, Ga/Y and Sn/Y. The solid black line indicates $T_1 = T_2$. The purple, blue, green and red dotted lines indicate T_1/T_2 of *n*-octane, ethanol, methanol and water imbibed within the pores of the specified catalyst, respectively. (For interpretation of the references to colour in this figure legend, the reader is referred to the web version of this article.)

the interaction with ethanol as opposed to methanol as seen from their T_1/T_2 values of 3.1 ± 0.1 and 2.8 ± 0.1, respectively. Although the difference is only small it is statistically significant and this implies that the zeolite surface adsorbs ethanol more strongly than methanol. When *n*-octane was used as a reference probe molecule, a T_1/T_2 value of 1.9 ± 0.1 was obtained. Due to its lack of chemical functionality, surface interactions with the zeolite will be limited and therefore, the motion of the molecule will be relatively fast when compared to the reaction solvents, thus leading to the low value observed.

It should be noted that the correlation plots obtained using methanol and ethanol as solvents show a second, less intense peak at approximately $T_1/T_2 \approx 7.1 \pm 0.2$, similar to that of the peak obtained in the water plot. This second peak contains signals from both OH species naturally present on the zeolite, such as adsorbed water and surface hydroxyls, and the OH moiety of the alcohol (methanol or ethanol). This is confirmed by the finding that the measured ratio of the peak areas does not reflect the aliphatic/OH ratios expected of the alcohol solvents and plots of the bare, non-soaked zeolites show a peak in the same position. Therefore, it is reasonable to assume that this second, less intense peak is due to the exchange of OH protons with adsorbed water protons and is not useful for the analysis. Hence, the analysis of this peak becomes ambiguous as it is not possible to separate the two proton environments in the relaxation domain. Therefore, the analysis of the main alkyl group peak of the alcohol is considered when calculating T_1/T_2. As for *n*-octane, the signal from water present within the zeolite is also present, however, this signal is not visible on the plot due to the overwhelming signal of *n*-octane protons.

The trend in relative adsorption strengths can be seen to be the same for both the metal doped zeolites and the parent zeolite. The results of all tests are summarized in Fig. 4 and numerically in Table S3.

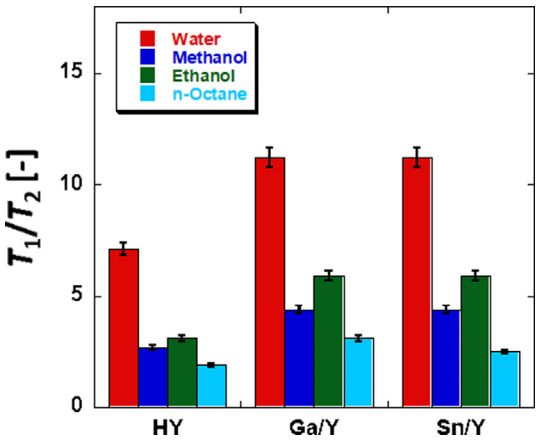

Fig. 4. T_1/T_2 of water, methanol, ethanol and *n*-octane imbibed within the pores of HY and metal doped derivatives Ga/Y and Sn/Y.

T_1/T_2 of water is shown to be the greatest across all samples indicating that, when imbibed within the pores of the zeolites, water exhibits the most reduced mobility. This can be attributed to the interaction of water with the zeolite surfaces (for example, through hydrogen bonding with surface hydroxyl groups). The relatively strong interaction of water with the catalyst surface will limit the accessibility of any reactants (in this case glucose and regardless of any conformation in solution [66]) to the active sites located on the catalyst surface, thereby resulting in a decreased catalytic activity, particularly if the active sites responsible for a reaction are located inside the pores of a zeolite. Additionally, the doped zeolites present a higher amount of Lewis centres (Sn^{4+} and Ga^{3+}) that can also coordinate H_2O, CH_3OH and CH_3CH_2-OH *via* the hydroxyl group and, in turn, also reduce their mobility leading to a site blocking effect when water is present.

Whilst the metal doped zeolites show higher T_1/T_2 when compared to that of the parent zeolite, it should be noted that T_1/T_2 can be affected by many other factors such as the presence of internal magnetic field gradients. Indeed, it has even been shown that T_2 values can differ significantly even for the same adsorbate in similar porous materials, [67] therefore this must be considered when comparing values across the different zeolite samples. However, this effect is most significant at high fields. In low-field benchtop instruments, such as that used in this study, they are less significant and a comparison across zeolites is reasonable.

Ga/Y and Sn/Y show higher T_1/T_2 for ethanol when compared to that of methanol, indicating that ethanol has a slightly stronger interaction with the zeolite surface. As discussed previously, the Lewis acid mediated sugar isomerization (forming fructose as the major product) is favoured in ethanol solvent, whereas the Brønsted acid mediated addition of the alcohol solvent (forming the alkyl fructoside as the major product) is favoured when methanol is used as the reaction solvent. Additionally, the Brønsted acid mediated pathway may not necessarily occur or be constrained by the zeolite pores, whereas the Lewis acid mediated pathway may be more prevalent within the pores of the zeolites. [38] As ethanol adsorbs relatively more strongly than methanol (as indicated by T_1/T_2), it is retained in the zeolite pores, along with any solvated products and reactant. As such, solvated fructose is preferentially prevented from further reaction on Brønsted acid sites outside of the pore whereas in methanol, the fructose produced can react on Brønsted acid sites outside of the pore resulting in an approximately equal distribution of reaction products as all reactive sites are accessible.

3.2.1. Control tests on framework and textural properties of the zeolites

We have characterized our materials using BET, porosimetry, and XRPD in order to demonstrate that no potential changes in the zeolite framework of our materials - resulting from their synthesis process - have occurred, which, in turn, has no impact on the NMR relaxation measurements reported above.

In fact, when metal centres are added to zeolites, the structure of the parent zeolites may change. This is a common occurrence when metal centres are added through ion-exchange methods, unlike the case of incipient wetness impregnation as a synthetic protocol, that was used in our study. [68–69].

Adsorption and desorption isotherms of N_2 at 77 K on HY, Sn/Y and Ga/Y (Figure S2) are consistent with types I and IV [70] with type-I typical of microporous materials (pore size < 2 nm), whereas type-IV is typical of materials presenting some mesoporous component (pore diameter between 2 nm and 50 nm). This is visible in hysteresis cycles exhibiting both condensation and cavitation. However, the short vertical hysteresis loops from p/p_0 = 0.5 to 0.99 indicate limited mesoporous volumes, as further confirmed by an analysis of pore distribution (Figures S3 and S4) where the materials are nearly exclusively microporous, centred at 0.74 nm and a mesoporous component between 20 and 40 nm.

An analysis of these isotherms by means of the Brunauer–Em mett–Teller (BET) model for the determination of specific surface areas, external and micropore areas, and the use of t-plots and a Horvarth-Kavazoe model for the pore volume and pore size distribution, respectively, led to the determination of the textural properties of our materials (Table 1).

It is possible to observe, that, within the experimental errors of our methods, all of these analyses revealed no changes in textural properties for any of our materials (all specific BET surface areas, external surface areas, and micropores are in the range of 700 m^2 g^{-1}, 450 m^2 g^{-1}, and 270 m^2 g^{-1}, respectively) except for a minor decrease in total surface area (around 12%) and pore volume (around 11%) when the metal dopant is added. This variation, on the other hand, is fully consistent with the use of an impregnation protocol as a deposition method, and it actually demonstrates the deposition of a metal dopant, mostly on the zeolite's external surface and close to the zeolites' pores.

In fact, no change in pore size or distribution before and after metal deposition, (Figures S3 and S4) nor changes in pressure in hysteresis cycles to induce condensation and cavitation, is observed, (Figure S2) and all materials present micropores with a cylindrical geometry of 7.4 Å diameter (Table 1 and Figure S3), as expected for a zeolite Y channel of 12 membered rings. [71] As a result, no actual change in the framework property, involving changes in the coordination or orientation of the zeolite's Al and Si centres, is present because of metal doping synthesis method.

To further reinforce this conclusion, we have characterized our materials by X-ray powder diffraction. Also in this case, by carrying out a Rietveld refinement on our X-ray patterns, (Table S4) no changes were detected, and all unit cell parameters before and after metal deposition (and even considering a sample as prepared for doping, but without metal dopant) are virtually identical, with a unit cell volume centred at 14363 $Å^3$ for all samples. Thus confirming that no change in framework properties occurred, including the absence of dealumination, and as such showing the framework is structurally resistant to our doping protocol.

3.2.2. Control tests on the effect of porosity on the reactivity of the zeolites

Aiming to specifically provide information on site blocking versus pore occupancy effects of the various solvents, as well as to assess the relevance of Brønsted acid sites, non-porous Sn-doped, Ga-doped, and un-doped SiO_2 and Al_2O_3 was synthesized and

Table 1
Textural properties of zeolites for the parent material (HY) and after metal doping (Sn/Y and Ga/Y) *via* an incipient impregnation protocol. Metal loading for both doped zeolites is 1 wt%.

Zeolite	Total surface area[(a)] ($m^2\ g^{-1}$)	External surface area[(a)] ($m^2\ g^{-1}$)	Micropore area[(a)] ($m^2\ g^{-1}$)	Pore volume[(b)] ($cm^3\ g^{-1}$)	Channel diameter[(c)] (Å)
HY	791 ± 18	499 ± 27	292 ± 16	0.261 ± 0.006	7.35 ± 0.05
Sn/Y	692 ± 16	421 ± 21	271 ± 14	0.222 ± 0.005	7.32 ± 0.04
Ga/Y	704 ± 16	444 ± 26	260 ± 16	0.231 ± 0.005	7.31 ± 0.06

[(a)] Values obtained from the adoption branch of the adsorption isotherms using Brunauer–Emmett–Teller (BET) theory.
[(b)] Value obtained at the absorption–desorption point using a Barret–Joyner–Halenda (BJH) method.
[(c)] Value obtained at the absorption–desorption point using a Horvath-Kawazoe method for a cylinder pore geometry.

tested to mimic the external surface of zeolites. This was done in order to explain differences in reactivity for this reaction as a function of the NMR relaxation data. In fact, whereas the pores of a zeolite could be subjected to both site blocking and pore occupancy effects, non-porous materials would be subjected to site blocking effects only.

The preparation method used herein (wet impregnation followed by calcination) to dope SiO_2 and Al_2O_3, leads to the formation of external SnO_2 and Ga_2O_3 clusters [68] (Figures S5 and S6, Table S5) thus also minimizing diffusion effects.

Sn/SiO_2, Sn/Al_2O_3, Ga/SiO_2, Ga/Al_2O_3 as well as SiO_2 and Al_2O_3 were tested for the isomerization reaction of glucose to fructose using water, methanol or ethanol as solvents (Table 2).

As found for the microporous zeolites, none of these non-porous materials, either doped or undoped showed any reactivity when water was used as a solvent. As such the lack of reactivity of zeolite Y based materials for the isomerization reaction is most probably due to both site blocking and pore occupancy effects affecting both Lewis and Brønsted centres.

This absence of reactivity shows consistency with the studies by Davis and co-workers on the activity of external SnO_2 clusters over zeolite beta, [72] whereby a lack of reactivity in water was also observed. Our tests would suggest this effect is more general and not necessarily restricted to zeolites having a particular structure, specific Sn-zeolite structures or metal clusters not necessarily limited to SnO_x clusters.

Comparison of these results using bulk supports to those from microporous zeolites Sn/Y and Ga/Y, prepared using the same impregnation protocol and metal loading (1 wt% as determined from ICP-MS measurements), and detailed characterization of these materials by means of XPS, HAADF-STEM and EXAF [40] showed that Sn/Y comprised SnO_2 clusters (average diameter 4.2 nm) outside the zeolite crystals and Ga/Y presented highly dispersed Ga_2O_3 species within the pores instead with evidence of some Ga substituted Al centres. This highlights the complexity of both the catalytic systems and the reactions that can take place on these catalysts, with a common denominator though, as in all these cases water always acts as an inhibitor for the isomerization reaction.

When using methanol as the reaction solvent, no activity was detected in the case of pure SiO_2, but this increased to 23 % and 11 % conversion when Sn/SiO_2 and Ga/SiO_2 were used as the catalyst, respectively. Furthermore, as there is no alkyl fructoside produced in any case, it can be concluded that the formation of alkyl fructose is inhibited by the absence of Brønsted acid sites which are present in all of the acid form zeolites that we used in this study (HY, Sn/Y and Ga/Y).

Control tests on metal leaching (Table S6) confirmed that any activity is not due to small amounts of these metals (< relative 1%) in solution, and, in turn, confirmed this activity is indeed due to Lewis Sn and Ga centres that are absent in pure SiO_2.

In the case of Al_2O_3, the bare oxide showed some activity (∼13 %) due to the presence of Lewis acid centres in Al_2O_3. This activity was further enhanced with the addition of Sn and Ga, thus leading to analogous considerations as those for doped non-porous SiO_2.

Table 2
Catalytic test results for the conversion of glucose to fructose and mannose using: Sn/SiO_2, Ga/SiO_2, Sn/Al_2O_3 and Ga/Al_2O_3 as control tests materials, and their supports: SiO_2 and γ-Al_2O_3 using different solvents: water, methanol and ethanol. In all cases, solutions containing 125 mg of glucose in 4 mL of solvents, were used at a reaction temperature of 100 °C and endogenous pressure. Metal loading for Sn and Ga was 1 wt% and the reactions were carried out at a constant molar metal to substrate ratio M:S = 1:100.

Catalyst	Solvent(s)	Conversion (%)	Selectivity (%)			CMB (%)
			Fructose	Mannose	R-F	
SiO_2	H_2O	0	n.d.	n.d.	n.d.	100
SiO_2	CH_3OH	0	n.d.	n.d.	n.d.	100
SiO_2	CH_3CH_2OH	0	n.d.	n.d.	n.d.	100
Sn/SiO_2	H_2O	0	n.d.	n.d.	n.d.	100
Sn/SiO_2	CH_3OH	23 ± 2	47 ± 3	53 ± 3	n.d.	96 ± 1
Sn/SiO_2	CH_3CH_2OH	21 ± 1	78 ± 1	23 ± 1	n.d.	88 ± 2
Ga/SiO_2	H_2O	0	n.d.	n.d.	n.d.	100
Ga/SiO_2	CH_3OH	11 ± 1	54 ± 1	46 ± 2	n.d.	100 ± 2
Ga/SiO_2	CH_3CH_2OH	19 ± 2	67 ± 3	33 ± 2	n.d.	100 ± 1
Al_2O_3	H_2O	0	n.d.	n.d.	n.d.	100
Al_2O_3	CH_3OH	13 ± 2	56 ± 1	44 ± 1	n.d.	100 ± 1
Al_2O_3	CH_3CH_2OH	23 ± 4	56 ± 2	44 ± 2	n.d.	88 ± 4
Sn/Al_2O_3	H_2O	0	n.d.	n.d.	n.d.	100
Sn/Al_2O_3	CH_3OH	30 ± 2	56 ± 3	44 ± 3	n.d.	91 ± 3
Sn/Al_2O_3	CH_3CH_2OH	27 ± 1	51 ± 1	49 ± 1	n.d.	83 ± 2
Ga/Al_2O_3	H_2O	0	n.d.	n.d.	n.d.	100
Ga/Al_2O_3	CH_3OH	19 ± 2	50 ± 1	50 ± 1	n.d.	90 ± 2
Ga/Al_2O_3	CH_3CH_2OH	23 ± 2	43 ± 3	57 ± 3	n.d.	92 ± 2

n.d. = not detected.
R-F = alkyl fructoside.

Regardless of the identity of the non-porous support used though, the activity is always significantly lower (5 to 10 times less) than in the presence of microporous zeolite HY. Therefore, it is possible to conclude that in the case of zeolites, the presence of pores is fundamental to drive the reaction and the isomerization reaction pathway does indeed occur inside the pores.

When ethanol is used as a solvent, similar results to those obtained using methanol were obtained, as this solvent can induce a small site blocking effect and as such, the reactivity on a porous zeolite will be dominated by pore occupancy. Also, in this case, no alkyl fructoside (obtained from Brønsted acidity) is detected but only the isomer fructose and the epimer mannose produced from Lewis acidity.

Conversion values appear to be the same or even higher than those obtained using methanol. Most likely due to ethanol being less protic and less nucleophilic than methanol, any site-blocking effect within the pores of the zeolites that could occur for water or methanol is even smaller when this solvent is used. It should also be noted, however, that specific considerations on possible nucleophilic effects of these solvents towards our substrates, are beyond the scope of the current study and therefore they are not being considered further. Though they may provide grounds for future investigations in this area.

The NMR relaxation measurements obtained provide indirect confirmation of these conclusions. In water, pores will be occluded by the limited mobility of the species within the pores and the Lewis sites will be blocked by strongly bound water molecules, the latter showing a very high strength of interaction as demonstrated by the T_1/T_2 values obtained. In contrast, as methanol is weakly adsorbed to the catalyst surface it will not block the pores of the zeolite, as well as not site-blocking its surface, and as such, allowing for a reaction to occur. At the same time though, the uptake of methanol and therefore solvated sugars into the zeolite pores will be relatively low when compared to ethanol. Therefore, the solvated sugars will interact with the Lewis acid sites and fructose will be formed as the major product.

T_1/T_2 obtained using *n*-octane confirmed that the difference in T_1/T_2 is due to differences in the surface interactions taking place between the reaction solvents and catalyst surfaces. Alkanes contain no functional groups and as such will have little or no interaction with the catalyst surface as for all the zeolite samples, *n*-octane shows the lowest value of T_1/T_2. As *n*-octane will not interact with the surface of the catalyst its mobility will be affected only by the structure and size of the catalyst pores. If no or weak interactions were taking place between the other solvents and the zeolite surfaces, all T_1/T_2 values obtained would be equivalent to that of *n*-octane. As this is clearly not the case, it can be concluded that the trend in T_1/T_2 seen is due to the adsorption of the solvent molecules to the zeolite surface.

3.3. 2D T_1-T_2 NMR solvent displacement

As these isomerization reactions may occur using different solvents either simultaneously or sequentially, [40] the displacement effect when changing solvent was examined. 2D T_1-T_2 NMR displacement experiments were performed to study the extent to which water blocked the pores/Lewis acid sites of the zeolites studied, as well as to determine how effectively ethanol and methanol can access the zeolite pores and the Lewis acid sites.

The displacement of methanol by water (Fig. 5a-5c) and the displacement of ethanol by water (Fig. 6a-6c), both showed a visible peak at T_1/T_2 = 7.1 ± 0.2 for HY (Fig. 5a and 6a) and at T_1/T_2 = 11 .2 ± 0.3 for the doped zeolites Ga/Y and Sn/Y (Fig. 5b, 5c, 6b and 6c respectively) in the correlation plots attributed to strongly adsorbed water present on the zeolite surfaces. At an experimental displacement time of 0 s, methanol/ethanol was present within the pores of the zeolite and the respective peaks can be clearly seen on the spectra. Again, it is important to clarify that the second alcohol peak seen was due to contributions of both the alcohol OH and water naturally present within the zeolite. With increasing displacement time, however, the alcohol peaks decrease in intensity and the water peak increases in intensity thus showing that water displaces the alcohol from the pores. After 600 s, methanol is completely displaced from the pores of the zeolites studied (Fig. 5a–5c) whereas a weak ethanol peak can still be seen (Fig. 6a–6c). This corroborates and supports the previous NMR relaxation experiments as ethanol was shown to adsorb more strongly to the zeolite surface than methanol (evidenced by the respective T_1/T_2 values) which, in turn, supports the catalytic data as the glucose isomerization reaction occurs readily in methanol and ethanol, but not at all in water. Additionally, a Lewis acid site catalyzed isomerization reaction inside the pores was favoured when ethanol was used.

To allow quantification of the solvent displacement experiments, the volume fractions of both water and the respective alcohol at each displacement time were determined. This analysis was performed by integration of both solvent peaks at each time point, and the volume fraction of each alcohol was determined using the following equation:

$$V_{Alc} = \frac{I_{Alc}}{I_{tot}} = \frac{I_{Alc}}{I_{Alc}+I_W}\# \quad (1)$$

where I_{Alc} is the integral of the alcohol peak and I_W is the integral of the water peak. To account for the water already strongly adsorbed to the zeolite surface (found to account for approximately 30% of the total integral), Equation (1) must be altered as follows:

$$V_{Alc} = \frac{I_{Alc}}{I_{Alc}+I_W-I_{W,0}}\# \quad (2)$$

where $I_{w,0}$ is the integral of the water peak at 0 s. Thus, leading to a variation in volume fraction of the alcohols imbibed within the pore of the zeolite samples with displacement time (Fig. 7).

With increasing displacement time both alcohols were displaced from the zeolite pores by water, as expected. Methanol was displaced significantly more rapidly than ethanol. For example, methanol was fully displaced from all zeolites by water after only 300 s, whereas ethanol remained in the pores (between 4 and 7 % of the total volume) after 600 s.

This can be attributed to the increased affinity of ethanol for the zeolite surface as previously determined from the T_1/T_2 values, making the displacement of ethanol molecules from the zeolite surface a slower process. This again supports the catalytic data and provides indirect confirmation that the Lewis acidic sites are located mainly within the zeolite pores.

As ethanol was more readily taken up and retained by the zeolite pores, the solvated sugars come into contact with the Lewis acidic centres located within the pores and the sugar isomerization pathway (Scheme 1) will be dominant. The solvated fructose was then retained by the pores and interacted weakly with Brønsted sites on the zeolite crystal surface, preventing the alcohol addition to form ethyl fructoside.

As methanol, instead, was only weakly adsorbed and not readily taken up by the zeolites pores, solvated sugars (namely fructose) were not retained by the zeolite pores and were able to interact with Brønsted sites on the outer surface of the zeolite crystal and form methyl fructoside, by the addition of methanol.

In contrast to the alcohol solvents, water completely blocks the zeolite pores and prevents access of the solvated glucose to the Lewis acid sites, therefore, the reaction was not able to progress.

The results herein are highly relevant with implications well beyond the reaction under study, especially when considering a large number of attempts in the literature aimed at using water

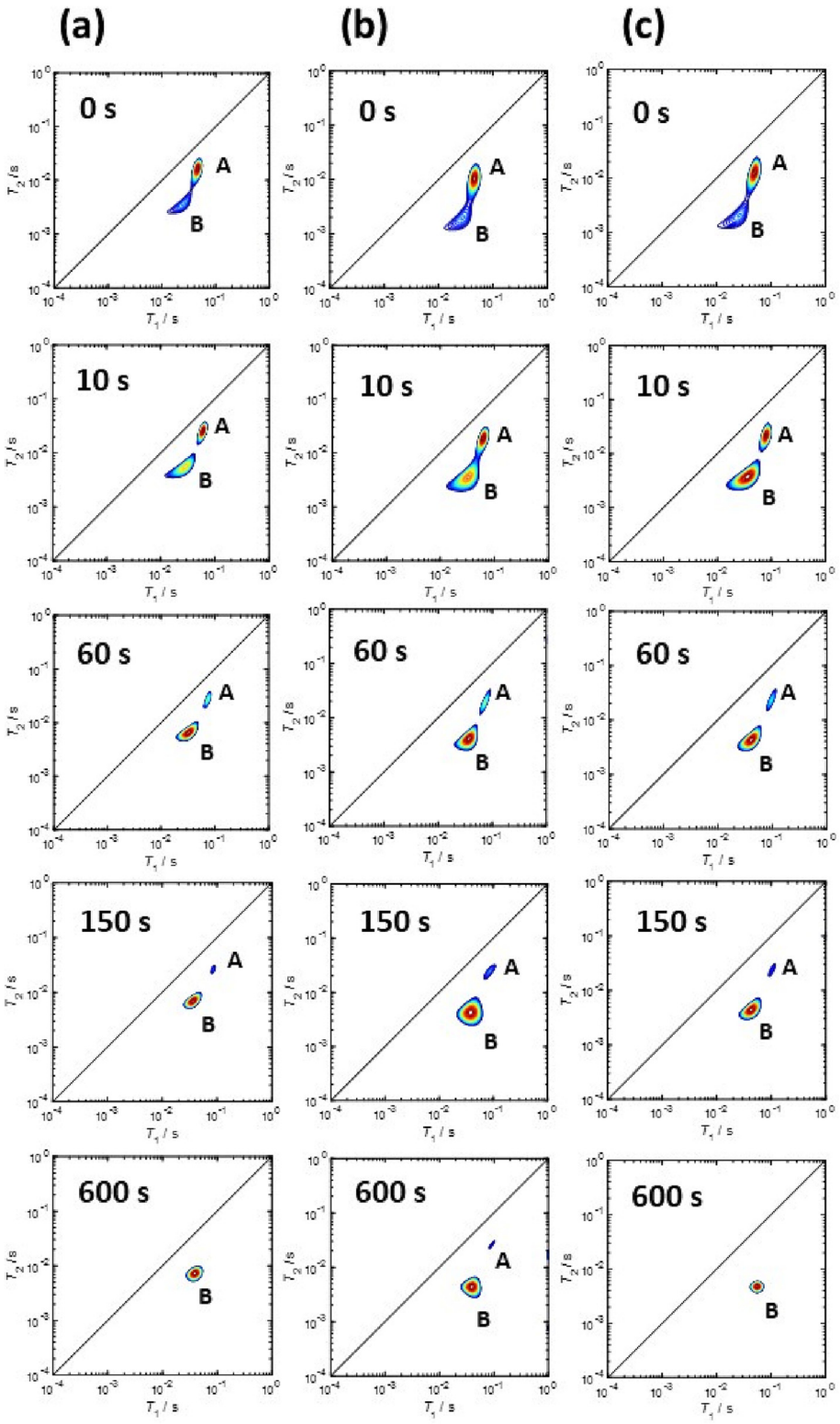

Fig. 5. T_1-T_2 relaxation correlation plots for methanol being displaced by water within the pores of (a) HY, (b) Ga/Y and (c) Sn/Y at the displacement time intervals of 0 s, 10 s, 60 s, 150 s and 600 s. A and B represent the aliphatic peak of the alcohol (methanol) and the OH/water peak, respectively.

as primary, environmentally friendly solvent, as from our experiments this may not be the best choice at a fundamental level.

3.4. Characterization of zeolite acidity

3.4.1. 2D T_1-T_2 pyridine and THF NMR relaxation

It has been widely reported how vital acidity is to the catalytic isomerization of glucose. [37,41] As the reaction mechanism in this study is found to be dependent upon the nature of the acid site

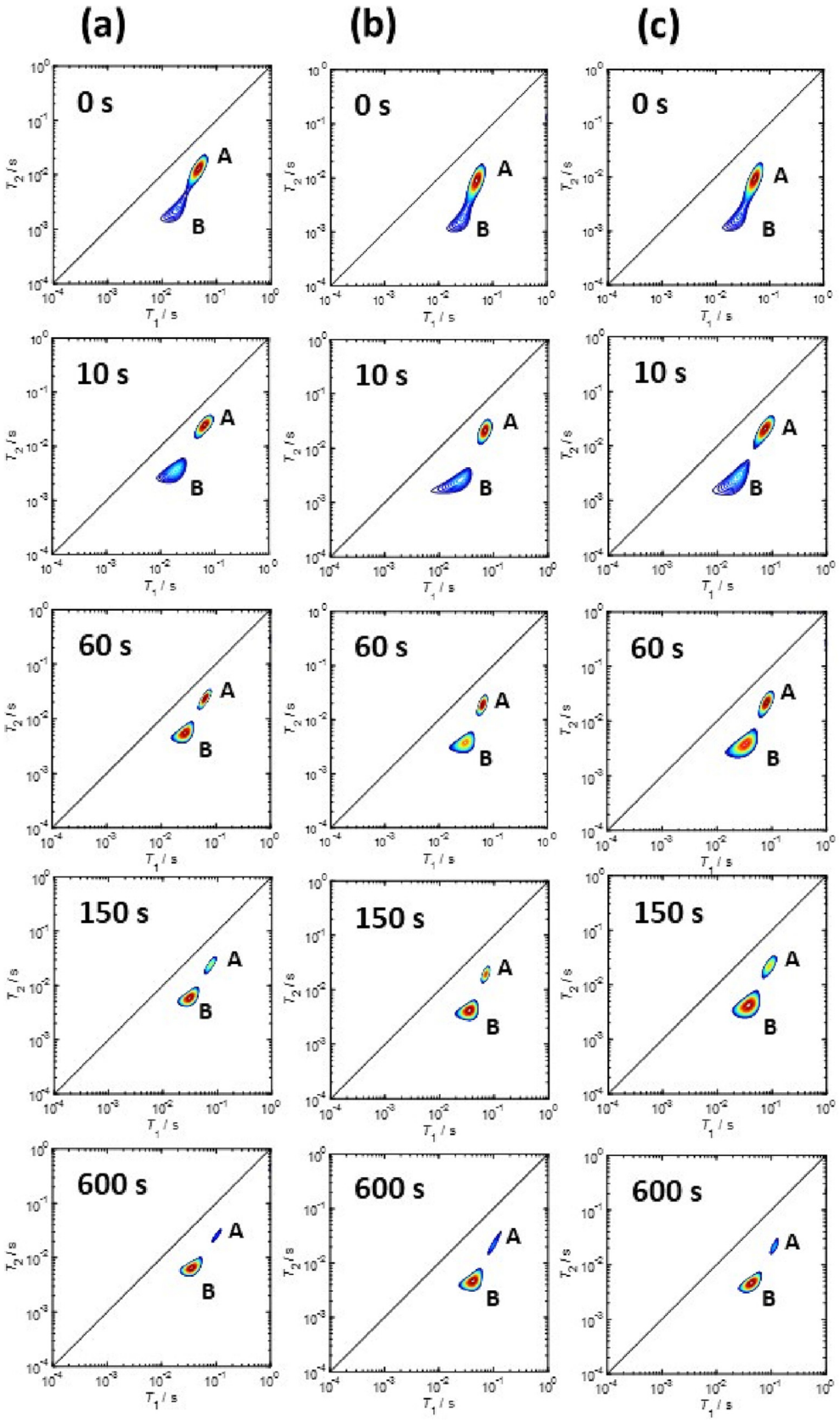

Fig. 6. T_1-T_2 relaxation correlation plots for ethanol being displaced by water within the pores of (a) HY, (b) Ga/Y and (c) Sn/Y at the displacement time intervals of 0 s, 10 s, 60 s, 150 s and 600 s. A and B represent the aliphatic peak of the alcohol (ethanol) and the OH/water peak, respectively.

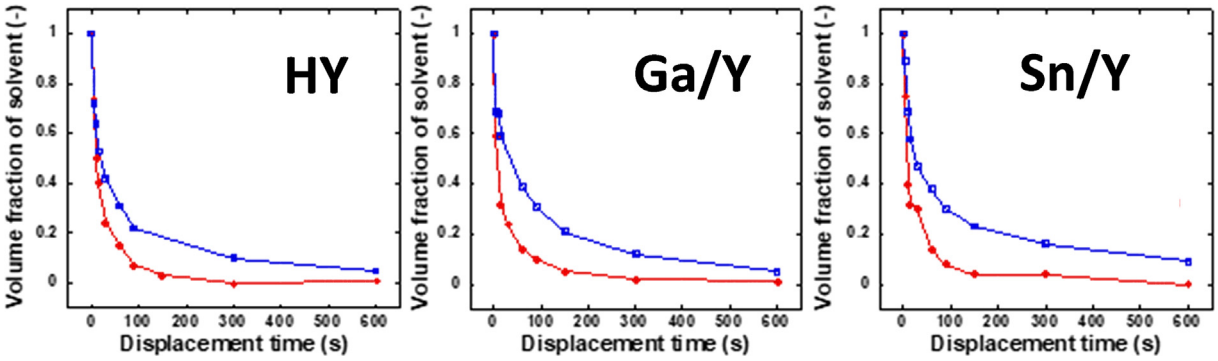

Fig. 7. The volume fraction of methanol (red line and data points) and ethanol (blue line and data points) remaining within the pores of HY, Ga/Y and Sn/Y during the displacement by water as a function of displacement time. The connecting lines are a guide to the eye. (For interpretation of the references to colour in this figure legend, the reader is referred to the web version of this article.)

involved (that is, Lewis sites within the pore and Brønsted sites external to the zeolite pores) which is, in turn, impacted by the solvent used, it seems appropriate to assess the nature of the zeolite acidity. Previous work has demonstrated that NMR relaxation time measurements using pyridine are a particularly effective way of characterizing the overall acid site strength of zeolites. [73–74] In brief, a higher T_1/T_2 measured for liquid pyridine molecules imbibed within the pores of said zeolite, indicates a higher relative strength of the strongest acid sites.

Herein, the use of tetrahydrofuran (THF) as a probe molecule for the Lewis acidity of catalytic materials has been examined. Whereas pyridine is both an effective Brønsted and Lewis base and, as such, can interact and probing both sources of catalyst acidity, THF is neither acidic nor basic in a Brønsted sense, but it is a relatively strong Lewis base. Therefore, THF should interact preferentially with Lewis acid sites on the zeolite surface and give an approximate indication of the relative strength of the zeolites overall Lewis acidity.

The results obtained from these measurements are reported in Figs. 8 and 9.

When pyridine adsorbed within the zeolite pores is considered, the determined T_1/T_2 values for HY and Ga/Y are not thought to be statistically different whilst that of Sn/Y is only slightly higher. That is, the calculated ratios of HY and Ga/Y imbibed with pyridine are approximately the same within experimental error. Therefore, it is reasonable to conclude that the overall acid site strength (that is a contribution by Brønsted and Lewis acid centres) is relatively unaffected by the presence of the metal dopants which is in excellent agreement with previously reported acidity data on these materials by multiple methods (back-titration and NH_3 chemisorption). [40].

Conversely, the results obtained using adsorbed THF as the probe molecule show a significant difference in the order of HY < Ga/Y < Sn/Y. That is, the strength of the THF-zeolite surface interaction increases in this order. This would suggest that the strength of the strongest Lewis acid sites on the zeolites is increased by the addition of the metal dopant and this increase in Lewis acid site strength is more pronounced for doping with Sn as opposed to Ga, but in both cases this is higher than the undoped HY material, thus showing that the metal doping does indeed increase the number of Lewis centres. This is a particularly interesting finding as measurements of catalyst Lewis acidity can be relatively complex and require the use of expensive equipment. Other similar techniques, such as solid state NMR using adsorbed phosphorous containing probe molecules trimethylphosphine (TMP) and trimethylphosphoneoxide (TMPO) have been previously reported as effective methods for acidity characterization in differing Lewis acid catalysts. [75–78] However, NMR relaxation measurements using THF represent a faster, cheaper and simpler method to probe the strength of Lewis acid sites at the expense of providing less information. That is, NMR relaxation methods cannot provide information on acid site locations, concentrations or spatial correlations. Therefore, the NMR relaxation methods reported do offer an important alternative technique for acidity characterization but the system, technique used and information required must be carefully considered.

3.4.2. Pyridine DRIFTS

To verify the results previously discussed, *in-situ* pyridine DRIFTS measurements were performed on the non-doped and metal-doped zeolites (Fig. 10 and Figures S7-S12). Peaks at *ca.* 1542 cm^{-1} and 1450 cm^{-1} are characteristic of Brønsted and Lewis acid sites, respectively, [79] involving the formation of pyridinium ions and weak adsorption interactions. In the region at 1490 cm^{-1}, it is possible instead to detect a combination of weaker Brønsted sites and stronger Lewis centres where pyridine will interact with both sites simultaneously. The presence of all three types of sites is detected in each sample, and it is these three peaks that are commonly used for the analysis of *in-situ* pyridine DRIFTS data. Following the adsorption of pyridine within the *in-situ* DRIFTS cell, a temperature programmed desorption (TPD) protocol was carried out from 50 °C to 350 °C in increments of 50 °C. The results of which can be seen in Fig. 10.

The DRIFTS spectra (Fig. 10) show the pyridine desorption process taking place as the intensity of each band decreases by differing amounts. Particularly, the Lewis and Brønsted bands (*ca.* 1450 cm^{-1} and 1542 cm^{-1}) reduce in intensity quite significantly. In addition to this, the bands appear to shift to higher wavenumbers (blue shift) which is indicative of an acid site of greater strength, as the wavenumber is directly proportional to the strength of the interaction of pyridine with the zeolite. [79] These results support the expected observation of more weakly bound molecules being removed from the surface at lower temperatures leaving only pyridine molecules bound to the strongest acid sites at the highest temperatures, as would be expected. To estimate the difference in acid site type in DRIFTS spectra, the Lewis-to-Brønsted population ratio (L/B) is commonly used by taking the ratio of the Lewis band intensity and the ratio of the Brønsted band intensity. L/B values were calculated for each catalyst at the various temperatures (Fig. 11, Tables S7-S9).

At the lowest temperature of 50 °C, there are clear differences in L/B between the three zeolites and with L/B of 1.4 – 2.3 it is clear that Lewis acidity is the dominant type of acid site. The L/B ratios increase in the order Sn/Y < Ga/Y < HY, the reverse order of the previously discussed NMR relaxation data. At temperatures above 150 °C, Brønsted acidity is dominant (L/B < 1), there are only small

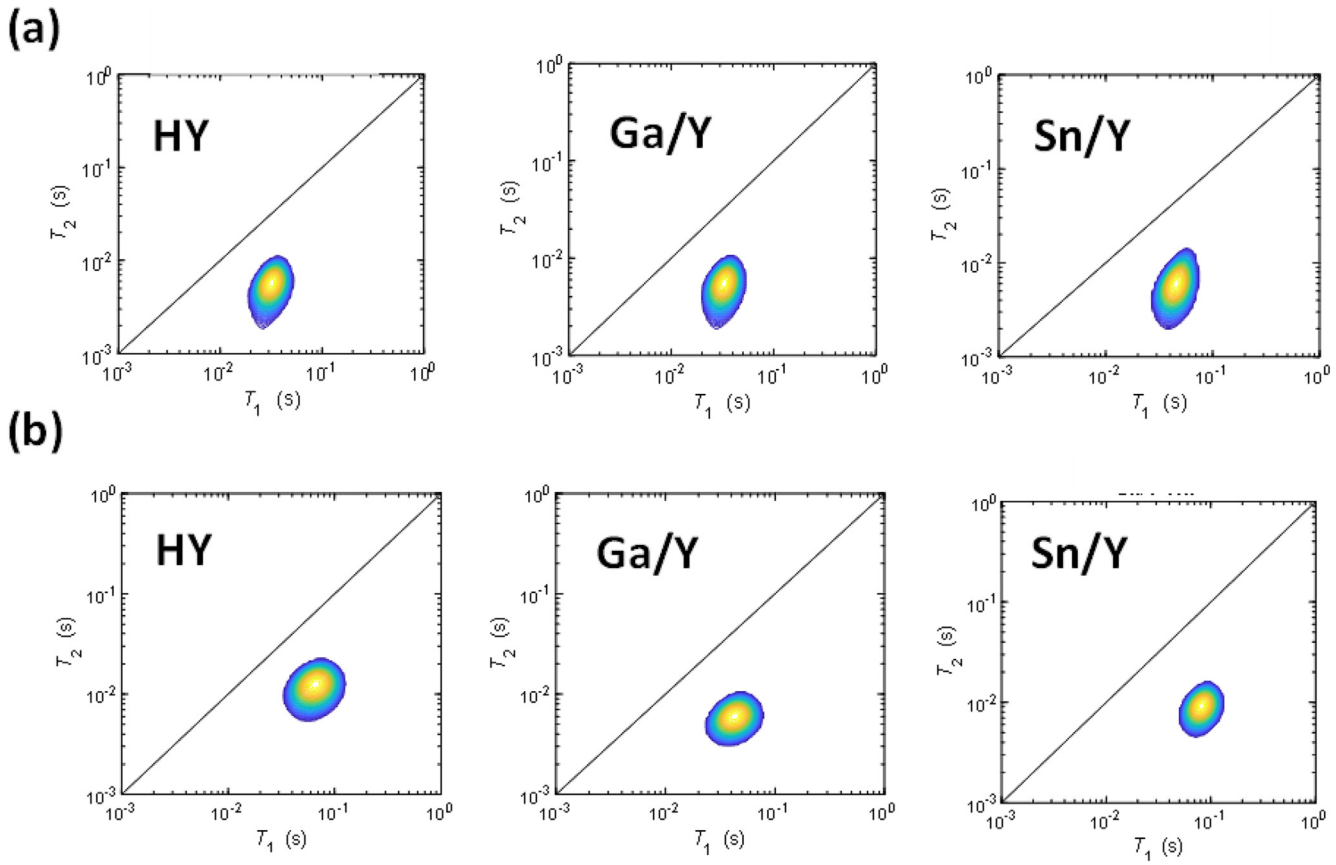

Fig. 8. T_1-T_2 relaxation correlation plots for (a) pyridine and (b) THF imbibed within the pores of the zeolites studied (the solid black line indicates $T_1 = T_2$).

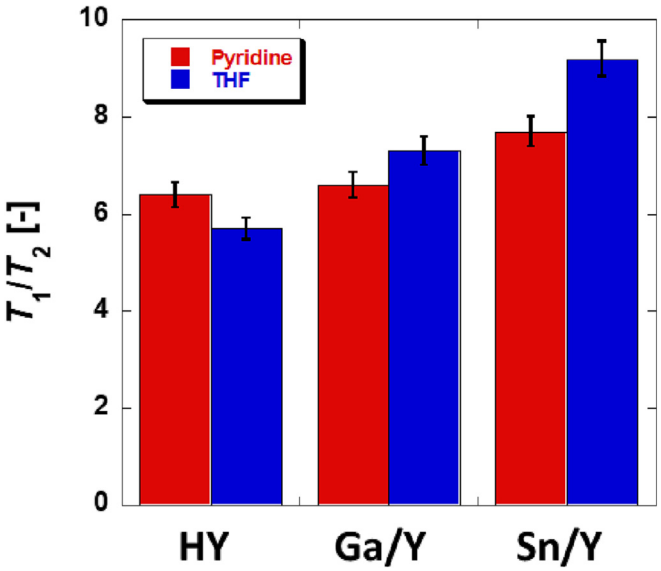

Fig. 9. T_1/T_2 values of pyridine and THF adsorbed within the pores of the zeolites studied. Pyridine is used to probe all acid sites on the catalyst surface and THF is used as a probe of Lewis acidity.

changes in L/B and the trend between zeolites is constant in the order of HY < Sn/Y < Ga/Y. The observed trend is typical for zeolites, it occurs in steam activation using residual moisture within the catalyst thereby creating more Brønsted acidity at the expense of Lewis acidity. Additionally, high temperatures may break ether-like bridges and form alcohols, which will further increase Brønsted acidity as Lewis acidity decreases. 150 °C is the highest temperature not to have residual moisture whilst avoiding the previously discussed material effects. Indeed, at this temperature L/B ~ 1 which is in excellent agreement with results from back titration and NH_3 chemisorption (ca. 0.7–0.8) from previous work. [40].

With the aim of validating both the NMR relaxation measurements (T_1/T_2) using both THF and pyridine and the *in-situ* pyridine-DRIFTS data (L/B), the correlation between the two factors was investigated. To simplify this analysis, T_1/T_2 values were converted to surface energies, e_{surf}, as reported elsewhere. [42] Essentially, the negative inverse of T_1/T_2 is representative of a characteristic surface energy for the imbibed molecule. In this case, e_{surf} represents the surface energy of the strongest acid site on the catalyst surface with which THF and pyridine can interact respectively (Table S10), as well as being used to correlate to L/B values (Fig. 12 for the temperatures of 50 °C, 100 °C and 150 °C).

At 50 °C and 100 °C, there is a relatively strong correlation between e_{surf} and the L/B ratio for both pyridine and THF. That is, as the L/B ratio increases so does the e_{surf} of the imbibed molecules (indicated by a more negative e_{surf} value). This correlation is more apparent when pyridine is used as opposed to THF. This is to be expected due to the consistency of using pyridine to measure L/B ratios *via* DRIFTS and NMR relaxation measurements. The correlation is less apparent when comparing pyridine-DRIFTS to THF-NMR. However, it is intriguing to see that such a relationship also exists when e_{surf} of THF is considered although to a lesser extent, likely as it mostly accounts for the Lewis acidity.

It is interesting to note that, e_{surf} of THF is greater than that of pyridine at relatively high L/B ratios whilst the opposite is true at lower L/B ratios. This would suggest that, at these temperatures of desorption, lower L/B ratios result in zeolites where the stron-

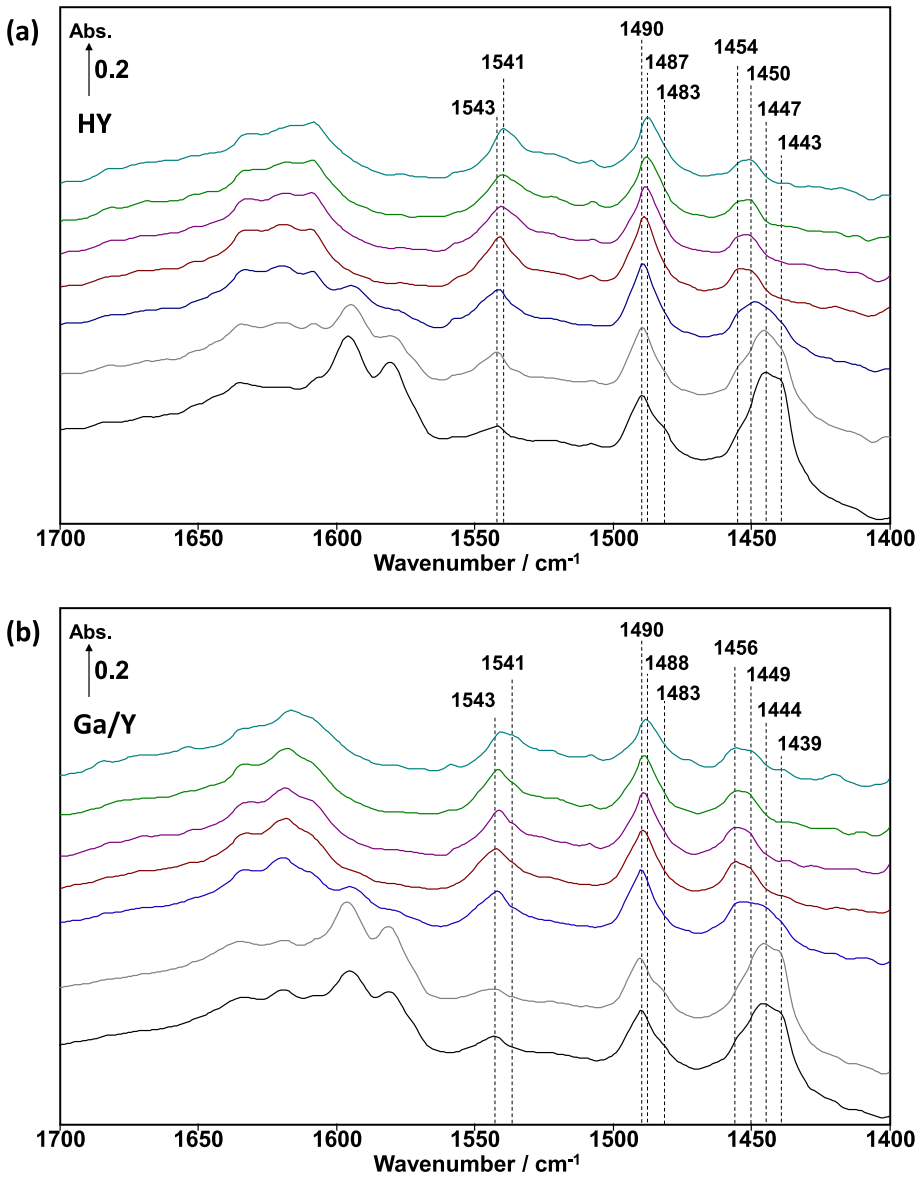

Fig. 10. DRIFTS spectra showing the desorption of pyridine from the surfaces of (a) HY, (b) Ga/Y and (c) Sn/Y. The temperature of the DRIFTS cell increased in increments of 50 °C up to 350 °C and *in-situ* DRIFTS spectra were acquired at each increment (50 °C, 100 °C, 150 °C, 200 °C, 250 °C, 300 °C, 350 °C). The temperature of desorption is increasing from the spectrum at the bottom to the spectrum at the top of the plot.

gest Lewis acid sites are weaker than the overall strongest acid sites on the zeolites surface. Conversely, when the L/B ratio is relatively high, Lewis acid sites are the strongest on the catalyst surface as indicated by the greater measured surface energy of THF, a molecule that is Lewis basic but not Brønsted basic.

This relationship does not persist at temperatures equal to or higher than 150 °C. This is to be expected as NMR relaxation/surface energy measurements were taken at room temperature, so as the analysis temperature further deviates from this temperature, relationships will become less relevant. It should also be noted that weaker acids that are not captured at higher desorption temperatures, may still be active at the reaction temperature used (100 °C). Additionally, Lewis and Brønsted acid sites are interconvertible at the reaction and desorption temperatures used in the presence of water. Both of these factors could contribute to a poor correlation between both techniques if higher desorption temperatures are considered.

4. Conclusions

In this paper, zeolite Y both non-doped in its acidic form HY, and doped with gallium and tin were tested as catalysts for the isomerization of glucose to fructose and mannose using three different solvents: water, methanol and ethanol. For each catalyst, no catalytic activity was observed in water. Conversely, glucose conversion was approximately 100 % when methanol and ethanol were used as the reaction solvents in a reaction mixture containing fructose, mannose and a methyl or an ethyl fructoside, respectively. However, when methanol was used as the reaction solvent, there was an approximately equal distribution of the three main reaction products for all the zeolites studied, in turn also showing a negligible effect on the catalytic activity by the metal dopant. This is probably due to a dominat Brønsted non-metal dependent reaction pathway. When ethanol was used, the major product produced was fructose for all three catalysts and according to a reaction pathway dominated by Lewis acid centres instead. These

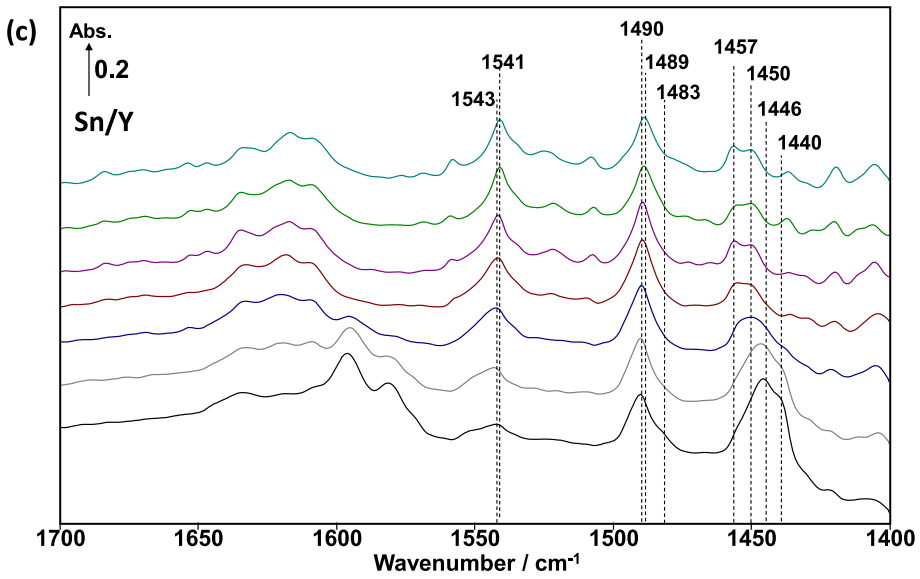

Fig. 10 (*continued*)

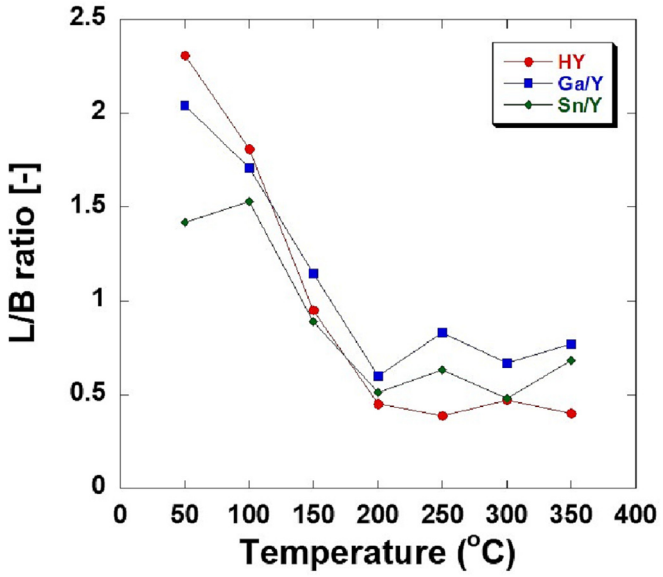

Fig. 11. The variation of the Lewis to Brønsted acid site ratio with desorption temperature within the *in-situ* DRIFTS cell.

results have major implications in terms of catalyst design for this important class of reactions. In fact, the reactivity and conversion of glucose to its various products is the result of two distinct reaction pathways: one is the direct isomerization of glucose to fructose and mannose that occurs inside the pores of the zeolites, and the other is fully dominated by Brønsted acidity that can also occur outside the pores, leading to alkyl fructoside and fructose by hydrolysis. As such, for the direct route a microporous material would be absolutely necessary whereas for the alkyl fructoside route this would not be the case.

2D NMR relaxation correlation measurements confirmed that methanol adsorbs the weakest to the zeolite surfaces and water adsorbs the strongest with ethanol intermediate between the two substantially altering the dominant reaction mechanism. This is consistent with the catalytic data, thus suggesting that the solvent effect is due to a blockage of active sites on the zeolite surface by the strong adsorption of water molecules. Ethanol adsorbs more strongly than methanol so it is more readily adsorbed into the zeolite pores where Lewis acidic centres can isomerize glucose to fructose. Methanol adsorbs more weakly, so solvated fructose is not retained by the pores and can preferentially react with Brønsted sites on the outer surface of the zeolite crystal forming methyl fructoside as the major product.

2D NMR displacement studies support the relaxation data as methanol is displaced from the zeolite pores by water more readily than ethanol. This is due to the stronger interactions between ethanol and the zeolite surface, making ethanol more difficult to dis-

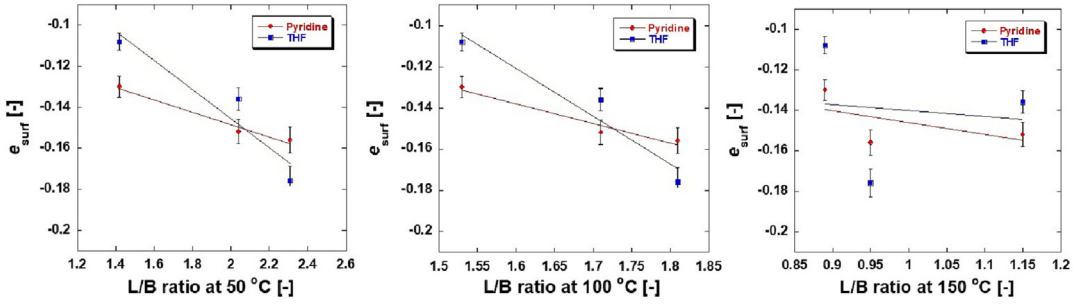

Fig. 12. The correlation between the Lewis to Brønsted acid site ratio at varying temperatures (50 °C, 100 °C, 150 °C) of desorption within the *in-situ* DRIFTS cell and e_{surf} across the range of the zeolites studied (*left*) HY, (*center*) Ga/Y and (*right*) Sn/Y. Red and blue points represent e_{surf} values determined from NMR using pyridine and THF respectively. (For interpretation of the references to colour in this figure legend, the reader is referred to the web version of this article.)

place from the zeolite pores than methanol which interacts with the zeolite surface more weakly.

In-situ pyridine-DRIFTS measurements resulted in Lewis to Brønsted ratios in excellent agreement with other techniques previously reported and showed a remarkable correlation with pyridine and THF surface energies calculated from the NMR relaxation results at temperatures equal to or below 100 °C. The correlation between NMR relaxation and pyridine DRIFTS measurements suggests that lower L/B ratios result in zeolites where the strongest Lewis acid sites are weaker than the overall strongest acid sites on the zeolites surface and vice versa when similar temperatures are used for both techniques.

To summarize, the study reported here, highlights the development and ways forward for an improved catalyst design of a moderately active, novel catalytic system to produce industrially valuable sugar compounds. The influence of the reaction solvent upon the overall catalytic activity was investigated using a low-field, benchtop NMR instrument, which is currently finding increasing use in the academic and industrial sectors as a relatively and simple technique to perform catalysis related studies such as the work described in this paper. Additionally, low-field NMR relaxation in combination with *in-situ* pyridine DRIFTS acidity measurements demonstrate an important tool to quantify the relative strengths of different catalyst acid sites as well as provide qualitative data on the types of catalyst sites present within the catalyst sample. Therefore, it is apparent that this work is of value not only to those working in the area of catalytic sugar isomerization but also to those investigating solvent effects and the influence of catalyst acidity in heterogeneous catalytic reactions and designing and optimizing heterogeneous catalytic processes.

CRediT authorship contribution statement

Luke Forster: Conceptualization, Methodology, Investigation, Writing – original draft, Formal analysis. **Mohamed M.M. Kashbor:** Methodology, Investigation, Formal analysis, Writing – review & editing. **James Railton:** Methodology, Investigation. **Sarayute Chansai:** Methodology, Investigation, Formal analysis, Writing – review & editing. **Christopher Hardacre:** Supervision, Funding acquisition, Writing – review & editing. **Marco Conte:** Conceptualization, Methodology, Investigation, Formal analysis, Visualization, Supervision, Funding acquisition, Writing – review & editing. **Carmine D'Agostino:** Conceptualization, Methodology, Visualization, Supervision, Funding acquisition, Writing – review & editing.

Data availability

Data will be made available on request.

Declaration of Competing Interest

The authors declare that they have no known competing financial interests or personal relationships that could have appeared to influence the work reported in this paper.

Acknowledgements

L.F., C. D. acknowledge the support of the Engineering Physical Sciences Research Council (EPSRC) (grant EP/V026089/1). M.M.M. K. acknowledges the support of the Libyan Ministry of Higher Education (grant CHM-345687), M.C. and J.R. acknowledge the support by the University of Sheffield (M.C. and J.R. CHM-316178). The authors thank Mr. Ben Palmer and Ms. Abby Shipley for their support at the department of Chemical and Biological Engineering at the University of Sheffield.

Appendix A. Supplementary material

Supplementary data to this article can be found online at https://doi.org/10.1016/j.jcat.2023.06.021.

References

[1] P.T. Anastas, J.C. Warner, Green Chemistry: Theory and Practice, Oxford University Press, 1998.
[2] P.T. Anastas, M.M. Kirchhoff, T.C. Williamson, Catalysis as a foundational pillar of green chemistry, Appl. Catal., A Gen. 221 (2001) 3–13.
[3] R.A. Sheldon, I. Arends, U. Hanefeld, Green Chemistry and Catalysis, Wiley-VCH, 2007.
[4] R.A. Sheldon, E factors, green chemistry and catalysis: An odyssey, ChemComm (2008) 3352–3365.
[5] P.T. Anastas, L.B. Bartlett, M.M. Kirchhoff, T.C. Williamson, The role of catalysis in the design, development and implementation of green chemistry, Catal. Today 55 (2000) 11–22.
[6] D.M. Alonso, J.Q. Bond, J.A. Dumesic, Catalytic conversion of biomass to biofuels, Green Chem. 12 (2010) 1493–1513.
[7] G. Baskar, R. Aiswarya, Trends in catalytic production of biodiesel from various feedstocks, Renew. Sustain. Energy Rev. 57 (2016) 496–504.
[8] B.H. Shanks, Conversion of biorenewable feedstocks: New challenges in heterogeneous catalysis, Ind. Eng. Chem. Res. 49 (2010) 10212–10217.
[9] H. Li, Z. Fang, R.L. Smith Jr, S. Yang, Efficient valorization of biomass to biofuels with bifunctional solid catalytic materials, Prog. Energy Combust. Sci. 55 (2016) 98–194.
[10] R.A. Sheldon, Green chemistry, catalysis and valorization of biomass, J. Mol. Catal. A Chem. 422 (2016) 3–12.
[11] C.M. Liu, S.Y. Wu, From biomass waste to biofuels and biomaterial building blocks, Renew. Energy 96 (2016) 1056–1062.
[12] L.E. Manzer, Catalytic synthesis of α-methylene-γ-valerolactone: A biomass-derived acrylic monomer, Appl. Catal. A Gen. 272 (2004) 249–256.
[13] W. Won, C.T. Maravelias, Thermal fractionation and catalytic upgrading of lignocellulosic biomass to biofuels: Process synthesis and analysis, Renew. Energy 114 (2017) 357–366.
[14] H.C. Ong, W.H. Chen, A. Farooq, Y.Y. Gan, K.T. Lee, V. Ashokkumar, Catalytic thermochemical conversion of biomass for biofuel production: A comprehensive overview, Renew. Sustain. Energy Rev. 113 (2019).
[15] M. Sajid, X. Zhao, D. Liu, Production of 2, 5-furandicarboxlylic acid (FDCA) from 5-hydroxymethylfurfural (HMF): Recent progress focusing on the chemical-catalytic routes, Green Chem. 20 (2018) 5427–5453.
[16] G. Yi, S.P. Teong, Y. Zhang, Base free conversion of 5-hydroxymethylfurfural to 2, 5-furandicarboxylic acid over a Ru/C catalyst, Green Chem. 18 (2016) 979–983.
[17] X. Han, C. Li, X. Liu, Q. Xia, Y. Wang, Selective oxidation of 5-hydroxymethylfurfural to 2, 5-furandicarboxylic acid over MnO_x-CeO_2 composite catalysts, Green Chem. 19 (2017) 996–1004.
[18] J. Shi, Y. Wang, X. Yu, W. Du, Z. Hou, Production of 2,5-dimethylfuran from 5-hydroxymethylfurfural over reduced graphene oxides supported Pt catalyst under mild conditions, Fuel 163 (2016) 74–79.
[19] Y. Zu, P. Yang, J. Wang, X. Liu, J. Ren, G. Lu, Y. Wang, Efficient production of the liquid fuel 2, 5-dimethylfuran from 5-hydroxymethylfurfural over Ru/Co_3O_4 catalyst, Appl Cat B Env. 146 (2014) 244–248.
[20] P. Yang, Q. Xia, X. Liu, Y. Wang, Catalytic transfer hydrogenation/hydrogenolysis of 5-hydroxymethylfurfural to 2, 5-dimethylfuran over Ni-Co/C catalyst, Fuel 187 (2017) 159–166.
[21] S. Chen, T. Maneerung, D.C.W. Tang, Y.S. Ok, C.H. Wang, Valorization of biomass to hydroxymethylfurfural, levulinic acid, and fatty acid methyl ester by heterogeneous catalysis, Chem. Eng. J. 328 (2017) 246–273.
[22] B. Chamnankid, C. Ratanatawanate, K. Faungnawakij, Conversion of xylose to levulinic acid over modified acid functions of alkaline-treated zeolite Y in hot-compressed water, Chem. Eng. J. 258 (2014) 341–347.
[23] Y. Shao, K. Sun, L. Zhang, Q. Xu, Z. Zhang, Q. Li, S. Zhang, Y. Wang, Q. Liu, X. Hu, Balanced distribution of Brønsted acidic sites and Lewis acidic sites for highly selective conversion of xylose into levulinic acid/ester over Zr-beta catalysts, Green Chem. 21 (2019) 6634–6645.
[24] X. Hu, C. Lievens, C.A. Larcher, C.Z. Li, Reaction pathways of glucose during esterification: Effects of reaction parameters on the formation of humin type polymers, Bioresource Technol. 102 (2011) 10104–10113.
[25] M.A. Mellmer, J.M.R. Gallo, D.M. Alonso, J.A. Dumesic, Selective production of levulinic acid from furfuryl alcohol in THF solvent systems over H-ZSM-5, ACS Catal. 5 (2015) 3354–3359.
[26] A. Onda, T. Ochi, K. Yanagisawa, Selective hydrolysis of cellulose into glucose over solid acid catalysts, Green Chem. 10 (2008) 1033–1037.
[27] S.G. Aspromonte, A. Romero, A.V. Boix, E. Alonso, Hydrolysis of cellulose to glucose by supercritical water and silver mesoporous zeolite catalysts, Cellulose 26 (2019) 2471–2485.
[28] J.R. Christianson, S. Caratzoulas, D.G. Vlachos, Computational insight into the effect of Sn-beta Na exchange and solvent on glucose isomerization and epimerization, ACS Catal. 5 (2015) 5256–5263.
[29] T. Ennaert, J. Van Aelst, J. Dijkmans, R. De Clercq, W. Schutyser, M. Dusselier, D. Verboekend, B.F. Sels, Potential and challenges of zeolite chemistry in the catalytic conversion of biomass, Chem. Soc. Rev. 45 (2016) 584–611.

[30] J. Faria, M.P. Ruiz, D.E. Resasco, Carbon nanotube/zeolite hybrid catalysts for glucose conversion in water/oil emulsions, ACS Catal. 5 (2015) 4761–4771.
[31] Y.P. Li, M. Head-Gordon, A.T. Bell, Analysis of the reaction mechanism and catalytic activity of metal-substituted beta zeolite for the isomerization of glucose to fructose, ACS Catal. 4 (2014) 1537–1545.
[32] Q. Yang, M. Sherbahn, T. Runge, Basic amino acids as green catalysts for isomerization of glucose to fructose in water, ACS Sustain. Chem. Eng. 4 (2016) 3526–3534.
[33] C.E. Crestani, A.T.C.R. Silva, A. Bernardo, C.B.B. Costa, M. Giulietti, Crystalline fructose production: a conceptual design with experimental data and operating cost analysis, Chem. Eng. Comm. 209 (2022) 869–881.
[34] J.-P. Lange, Performance metrics for sustainable catalysis in industry, Nature Catal. 4 (2021) 186–192.
[35] M. Moliner, Y. Román-Leshkov, M.E. Davis, Tin-containing zeolites are highly active catalysts for the isomerization of glucose in water, Proc. Natl. Acad. Sci. USA 107 (2010) 6164.
[36] A. Corma, Inorganic solid acids and their use in acid-catalyzed hydrocarbon reactions, Chem. Rev. 95 (1995) 559–614.
[37] R. Bermejo-Deval, M. Orazov, R. Gounder, S.J. Hwang, M.E. Davis, Active sites in Sn-Beta for glucose isomerization to fructose and epimerization to mannose, ACS Catal. 4 (2014) 2288–2297.
[38] R. Gounder, M.E. Davis, Monosaccharide and disaccharide isomerization over Lewis acid sites in hydrophobic and hydrophilic molecular sieves, J. Catal. 308 (2013) 176–188.
[39] R. Gounder, M.E. Davis, Beyond shape selective catalysis with zeolites: Hydrophobic void spaces in zeolites enable catalysis in liquid water, AIChE J. 59 (2013) 3349–3358.
[40] M.M.M. Kashbor, D. Sutarma, J. Railton, N. Sano, P.J. Cumpson, D. Gianolio, G. Cibin, L. Forster, C. D'Agostino, X. Liu, L. Chen, V. Degirmenci, M. Conte, Conversion of glucose to fructose over Sn and Ga-doped zeolite Y in methanol and water media, Appl. Catal. A Gen. 642 (2022).
[41] S. Saravanamurugan, M. Paniagua, J.A. Melero, A. Riisager, Efficient isomerization of glucose to fructose over zeolites in consecutive reactions in alcohol and aqueous media, J. Am. Chem. Soc. 135 (2013) 5246–5249.
[42] C. D'Agostino, J. Mitchell, M.D. Mantle, L.F. Gladden, Interpretation of NMR relaxation as a tool for characterising the adsorption strength of liquids inside porous materials, Chem. Eur. J. 20 (2014) 13009–13015.
[43] C. D'Agostino, G.L. Brett, P.J. Miedziak, D.W. Knight, G.J. Hutchings, L.F. Gladden, M.D. Mantle, Understanding the solvent effect on the catalytic oxidation of 1, 4-butanediol in methanol over Au/TiO_2 catalyst: NMR diffusion and relaxation studies, Chem. Eur. J. 18 (2012) 14426–14433.
[44] C. D'Agostino, M.R. Feaviour, G.L. Brett, J. Mitchell, A.P.E. York, G.J. Hutchings, M.D. Mantle, L.F. Gladden, Solvent inhibition in the liquid-phase catalytic oxidation of 1, 4-butanediol: Understanding the catalyst behaviour from NMR relaxation measurements, Catal. Sci. Technol. 6 (2016) 7896–7901.
[45] C. D'Agostino, T. Kotionova, J. Mitchell, P.J. Miedziak, D.W. Knight, S.H. Taylor, G.J. Hutchings, L.F. Gladden, M.D. Mantle, Solvent effect and reactivity trend in the aerobic oxidation of 1, 3-propanediols over gold supported on titania: NMR diffusion and relaxation studies, Chem. Eur. J. 19 (2013) 11725–11732.
[46] C. D'Agostino, M.D. Mantle, L.F. Gladden, Inhibitory effect of oxygenated heterocyclic compounds in mesoporous catalytic materials: A pulsed-field gradient NMR diffusion study, Microporous Mesoporous Mater 269 (2018) 88–92.
[47] L. Forster, Z. Qie, M. Hu, A. Mavridis, C. Price, C.M.A. Parlett, X. Fan, C. D'Agostino, Heteropolyacids supported on zirconia-doped γ, θ and α alumina: A physicochemical assessment and characterisation of supported solid acids, Appl. Surf. Sci. 605 (2022).
[48] V.J. Witherspoon, R. Mercado, E. Braun, A. Mace, J. Bachman, J.R. Long, B. Blümich, B. Smit, J.A. Reimer, Combined nuclear magnetic resonance and molecular dynamics study of methane adsorption in M_2(dobdc) metal-organic frameworks, J. Phys. Chem. C 123 (2019) 12286–12295.
[49] H. Mao, J. Tang, J. Xu, Y. Peng, J. Chen, B. Wu, Y. Jiang, K. Hou, S. Chen, J. Wang, H.R. Lee, D.M. Halat, B. Zhang, W. Chen, A.Z. Plantz, Z. Lu, Y. Cui, J.A. Reimer, Revealing molecular mechanisms in hierarchical nanoporous carbon via nuclear magnetic resonance, Matter 3 (2020) 2093–2107.
[50] B. Dinakar, A.C. Forse, H.Z.H. Jiang, Z. Zhu, J.-H. Lee, E.J. Kim, S.T. Parker, C.J. Pollak, R.L. Siegelman, P.J. Milner, J.A. Reimer, J.R. Long, Overcoming metastable CO_2 adsorption in a bulky diamine-appended metal-organic framework, J. Am. Chem. Soc. 143 (2021) 15258–15270.
[51] L. Qi, R. Alamillo, W.A. Elliott, A. Andersen, D.W. Hoyt, E.D. Walter, K.S. Han, N. M. Washton, R.M. Rioux, J.A. Dumesic, S.L. Scott, Operando solid-state NMR observation of solvent-mediated adsorption-reaction of carbohydrates in zeolites, ACS Catal. 7 (2017) 3489–3500.
[52] M.J. Cordon, J.W. Harris, J.C. Vega-Vila, J.S. Bates, S. Kaur, M. Gupta, M.E. Witzke, E.C. Wegener, J.T. Miller, D.W. Flaherty, D.D. Hibbitts, R. Gounder, Dominant role of entropy in stabilizing sugar isomerization transition states within hydrophobic zeolite pores, J. Am. Chem. Soc. 140 (2018) 14244–14266.
[53] M. Conte, J.A. Lopez-Sanchez, Q. He, D.J. Morgan, Y. Ryabenkova, J.K. Bartley, A. F. Carley, S.H. Taylor, C.J. Kiely, K. Khalid, G.J. Hutchings, Modified zeolite ZSM-5 for the methanol to aromatics reaction, Catal. Sci. Technol. 2 (2012) 105–112.
[54] R.J. Hill, M.D. Cranswick, International Union of Crystallography. Commission on powder diffraction. Rietveld refinement round robin. II. Analysis of monoclinic ZrO_2, J. Appl. Cryst. 24 (1994) 802–844.
[55] F. Sánchez-Bajo, F.L. Cumbrera, A Gaussian-Hermite polynomials function for X-ray diffraction profile fitting, J. Appl. Cryst. 32 (1999) 730–735.
[56] Crystallographic information files made by reference to http://www.izastructure.org/databases/.
[57] K. Sing, The use of nitrogen adsorption for the characterisation of porous materials, Colloids Surf., A 187–188 (2001) 3–9.
[58] E.P. Barrett, L.G. Joyner, P.P. Halenda, The determination of pore volume and area distributions in porous substances. I. Computations from nitrogen isotherms, J. Am. Chem. Soc. 73 (1951) 373–380.
[59] A. Galarneau, D. Desplantier, R. Dutartre, F. Di Renzo, Micelle-templated silicates as a test bed for methods of mesopore size evaluation, Microporous Mesoporous Mater. 27 (1999) 297–308.
[60] V. Sebastián, C. Casado, J. Coronas, Special applications of zeolites, in: Zeolites and Catalysis: Synthesis, Reactions and Applications, 1st ed.;., Wiley-VCH, 2010, pp. 389–410.
[61] G. Filippini, F. Longobardo, L. Forster, A. Criado, G. Di Carmine, L. Nasi, C. D'Agostino, M. Melchionna, P. Fornasiero, M. Prato, Light-driven, heterogeneous organocatalysts for C-C bond formation towards valuable perfluoroalkylated intermediates, Sci. Adv. 6 (2020) eabc9923.
[62] N.S. Gould, S. Li, H.J. Cho, H. Landfield, S. Caratzoulas, D. Vlachos, P. Bai, B. Xu, Understanding solvent effects on adsorption and protonation in porous catalysts, Nat. Commun. 11 (2020) 1060.
[63] K.-J. Dunn, Enhanced transverse relaxation in porous media due to internal field gradients, J. Magn. Reson. 156 (2002) 171–180.
[64] J. Mitchell, T.C. Chandrasekera, M.L. Johns, L.F. Gladden, Nuclear magnetic resonance relaxation and diffusion in the presence of magnetic field gradients: The effect of magnetic field strength, Phys. Rev. E 81 (2010).
[65] J.-P. Korb, Multiscale nuclear magnetic relaxation dispersion of complex liquids in bulk and confinement, Prog. Nucl. Magn. Reson. Spectrosc. 104 (2018) 12–55.
[66] Y. Kim, A. Mittal, D.J. Robichaud, H.M. Pilath, B.D. Etz, P.C. St John, D.K. Johnson, S. Kim, Prediction of hydroxymethylfurfural yield in glucose conversion through investigation of Lewis acid and organic solvent effects, ACS Catal. 10 (2020) 14707–14721.
[67] J. Mitchell, S. Stark, J.H. Strange, Probing surface interactions by combining NMR cryoporometry and NMR relaxometry, J. Phys. D 38 (2005) 1950–1958.
[68] J.A. Lopez-Sanchez, M. Conte, P. Landon, W. Zhou, J.K. Bartley, S.H. Taylor, A.F. Carley, C.J. Kiely, K. Khalid, G.J. Hutchings, Reactivity of Ga_2O_3 clusters on zeolite ZSM-5 for the conversion of methanol to aromatics, Cat. Lett. 142 (2012) 1049–1056.
[69] C. Flores, N. Batalha, N.R. Marcilio, V.V. Ordomsky, A.Y. Khodakov, Influence of impregnation and ion exchange sequence on metal localization, acidity and catalytic performance of cobalt BEA zeolite catalysts in Fischer-Tropsch synthesis, ChemCatChem 11 (2019) 568–574.
[70] F.N. Ridha, Y. Yang, P.A. Webley, Adsorption characteristics of a fully exchanged potassium chabazite zeolite prepared from decomposition of zeolite Y, Microporous Mesoporous Mater. 117 (2009) 497–507.
[71] F.C. Hendriks, D. Valencia, P.C.A. Bruijnincx, B.M. Weckhuysen, Zeolite molecular accessibility and host-guest interactions studied by adsorption of organic probes of tunable Size, Phys. Chem. Chem. Phys. 19 (2017) 1857–1867.
[72] R. Bermejo-Deval, G. Gounder, M.E. Davis, Framework and extraframework tin sites in zeolite beta react glucose differently, ACS Catal. 2 (2012) 2705–2713.
[73] N. Robinson, P. Bräuer, A.P.E. York, C. D'Agostino, Nuclear spin relaxation as a probe of zeolite acidity: A combined NMR and TPD investigation of pyridine in HZSM-5, Phys. Chem. Chem. Phys. 23 (2021) 17752–17760.
[74] C. D'Agostino, A.P.E. York, P. Bräuer, Host-guest interactions and confinement effects in HZSM-5 and chabazite zeolites studied by low-field NMR spin relaxation, Mater. Today Chem. 24 (2022).
[75] A. Zheng, S.-J. Huang, S.-B. Liu, F. Deng, Acid properties of solid acid catalysts characterized by solid-state ^{31}P NMR of adsorbed phosphorous probe molecules, Phys. Chem. Chem. Phys. 13 (2011) 14889–14901.
[76] X. Yi, H.-H. Ko, F. Deng, S.-B. Liu, A. Zheng, Solid state ^{31}P NMR mapping of active centers and relevant spatial correlations in solid acid catalysts, Nat. Protoc. 15 (2020) 3527–3555.
[77] Y. Koito, K. Nakajima, R. Hasegawa, H. Kobayashi, M. Kitano, M. Hara, Lewis acid properties of some metal salts for lactic acid formation in water: ^{31}P NMR spectroscopy with trimethylphosphine oxide as a molecular probe, Catal. Today 226 (2014) 198–203.
[78] D. Rivera-Barrera, J.C. Poveda-Jaramillo, Thermal desorption of trimethylphosphine (TMP) on the HY zeolite followed by FT-IR and ^{31}P MAS NMR, J. Solid State Chem. 294 (2021).
[79] A. Platon, W.J. Thomson, Quantitative Lewis/Brønsted ratios using DRIFTS, Ind. Eng. Chem. Res. 42 (2003) 5988–5992.